18 Gas Turbine Engines, Design and Dynamic Performance

A gas turbine engine is a system that consists of several turbomachinery components and auxiliary subsystems. Air enters the compressor component which is driven by a turbine component and is placed on the same shaft. Air exits the compressor at a higher pressure and enters the combustion chamber, where the chemical energy of the fuel is converted into thermal energy producing combustion gas at a temperature that corresponds to the turbine inlet design temperature. The combustion gas expands in the following turbine component, where its total energy is partially converted into shaft work and exit kinetic energy. For power generation gas turbines, the shaft work is the major portion of the above energy forms. It covers the total work required by the compressor component, the bearing frictions, several auxiliary subsystems, and the generator. In aircraft gas turbines, a major portion of the total energy goes toward generation of high exit kinetic energy that is essential for thrust generation.

Gas turbines are designed for particular applications that determine their design configurations. For power generation purposes, the gas turbine usually has a *single spool*. A spool combines a compressor and a turbine that are connected together via

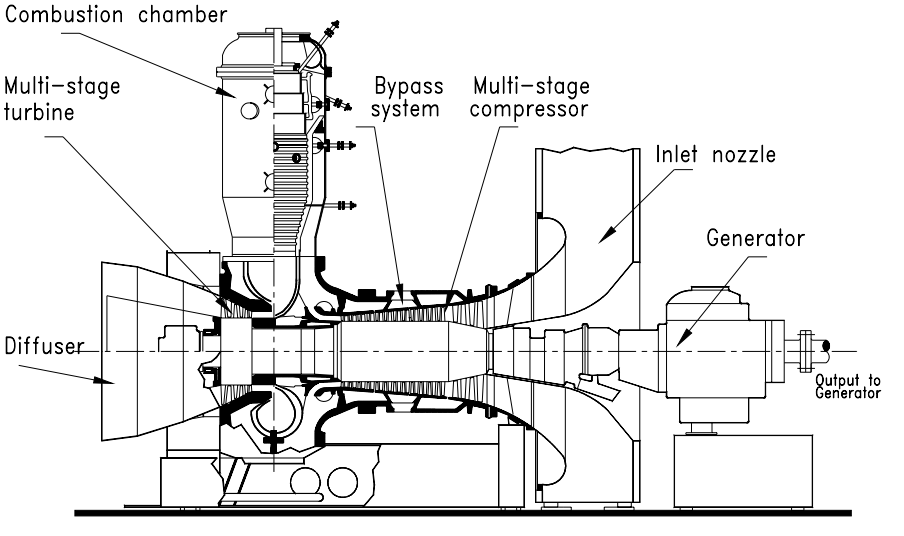

Fig. 18.1: A single-spool power generation gas turbine, BBC-GT9

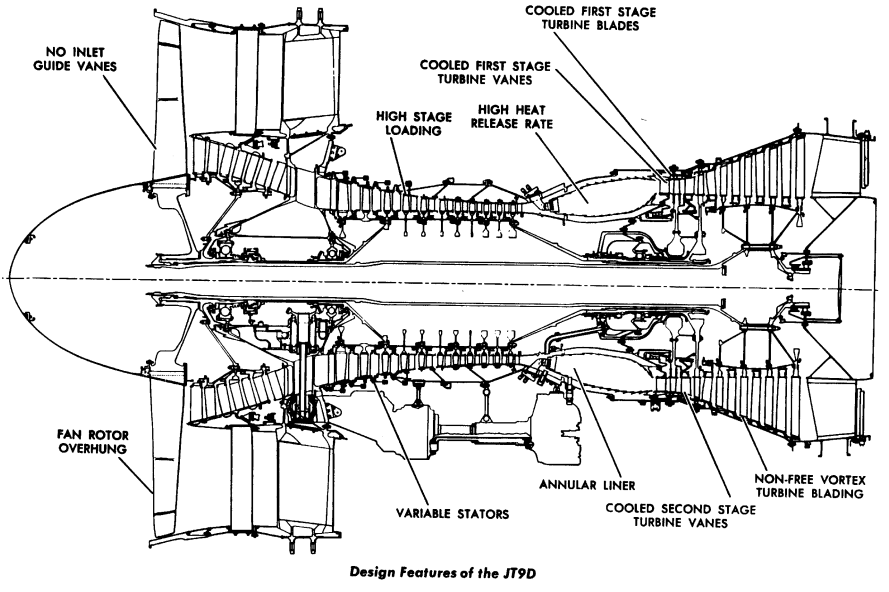

Fig. 18.2: A twin-spool Pratt & Whitney high bypass ratio aircraft engine with multi-stage compressors and turbines

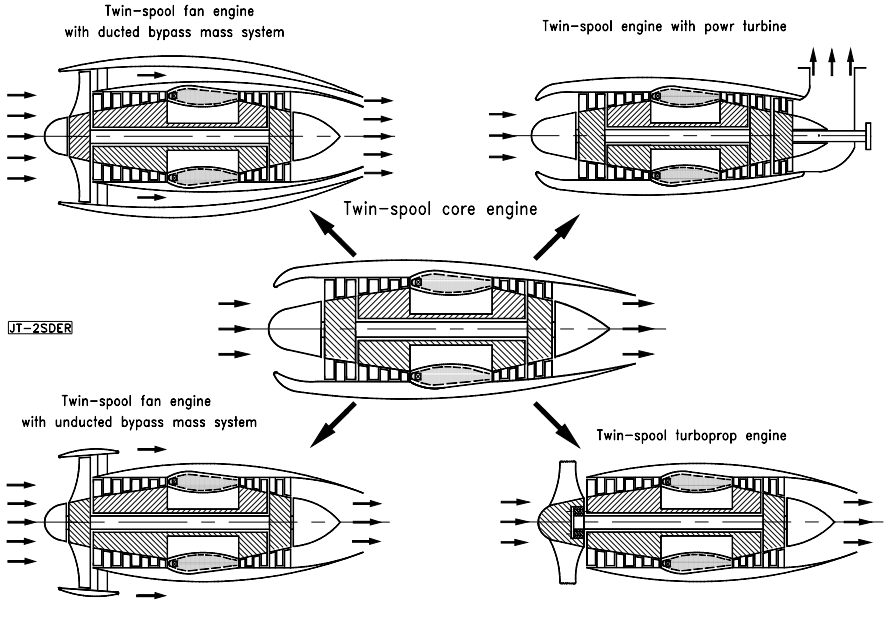

Fig. 18.3: Schematic of a twin-spool core engine with its derivatives

a shaft. Fig. 18.1 exhibits a single-spool power generation gas turbine, where a 14-stage compressor shares the same shaft with a 3-stage turbine.

While in power generation gas turbine design the power/weight ratio does not play an important role, the thrust/weight ratio is a primary parameter in designing an aircraft gas turbine. High performance aircraft gas turbine engines generally have twin-spool or multi-spool arrangements. The spools are usually rotating at different angular velocities and are connected with each other aerodynamically via air or combustion gas. Fig. 18.2 exhibits a typical high performance twin spool aircraft gas turbine with a *ducted front fan* as the main thrust generator. Gas turbine engines with power capacities less than 20 MW might have a *split shaft* configuration that consists of a *gas generation spool* and a *power shaft*. While the turbine of the gas generation spool provides the necessary shaft work to drive the compressor, the power shaft produces the net power. In addition to the above design configurations, a variety of engine derivatives can be constructed using a core engine as shown in Fig. 18.3.

18.1 Gas Turbine Steady Design Operation, Process

Starting with the single-spool power generation gas turbine that consists of a multi-stage compressor, a combustion chamber, and a turbine, the h-s diagram is shown in Fig. 18.4(a).

The compression process from 1 to 2 is accomplished by the compressor with a polytropic efficiency η_{pol} that can be accurately calculated using the row-by-row or stage-by-stage methods discussed in Chapters 16. The combustion process from 2 to 3 is associated with certain total pressure loss coefficient ζ_{comb} thus, it is not

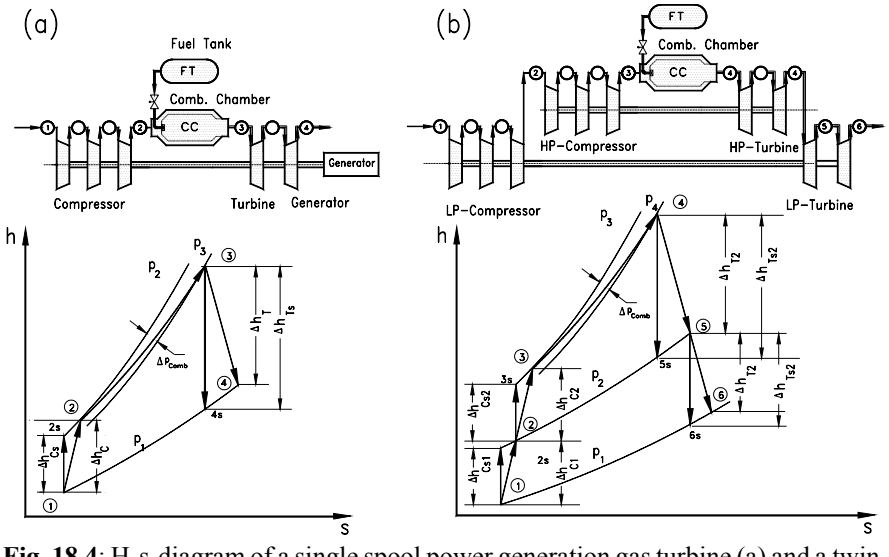

Fig. 18.4: H-s-diagram of a single spool power generation gas turbine (a) and a twin-spool aircraft engine (b)

considered isobaric. The expansion process from 3 to 4 causes an entropy increase that is determined by the turbine efficiency. Figure 18.4(b) shows the h-s diagram for a twin spool aircraft engine. In contrast to the single spool engine, the compression process is accomplished by two compressors that are operating at two different angular velocities. Air enters the low pressure compressor (LP-compressor) driven by the LP-turbine and is compressed from 1 to 2. Further compression from 2 to 3 occurs in the high pressure compressor (HP-compressor) driven by the HP-turbine. After addition of fuel in the combustion chamber, fist expansion occurs in the HP-turbine, whose power exactly matches the sum of HP-compressor power and the power required to compensate bearing frictions. Second expansion in LP-turbine matches the power by the LP-compressor, bearing friction, and the auxiliary subsystems. In off-design operation, there is always a dynamic mismatch between the turbine and compressor power that changes the spool rotational speed. This dynamic mismatch is brought to an equilibrium by taking appropriate control measures, as we discuss in the following sections. As mentioned briefly, small gas turbines may have a split shaft configuration as shown in Fig. 18.5. The single spool gas generator unit provides the power turbine with combustion gas that has the required pressure and temperature to produce the power. As seen in Fig. 18.5(a), the specific turbine enthalpy difference is $\Delta h_T \approx \Delta h_C$, leaving the rest enthalpy difference Δh_{PT} for power generation.

Figure 18.5(b) shows the h-s diagram of a high efficiency power generation gas turbine. The schematic cross section of this gas turbine is shown in Fig. 18.9. It consists of a multi-stage compressor, *C*, a combustion chamber, *CC1*, providing a lean combustion gas that expands in a single-stage reheat turbine, *RT*. The exhaust gas from *RT* enters the second combustion chamber, *CC2*, where the remaining fuel

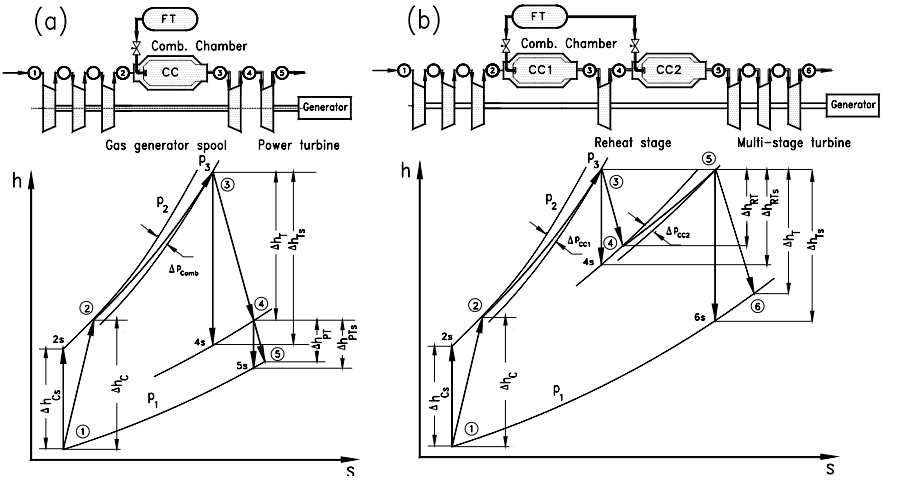

Fig. 18.5: H-s-diagram of a single spool power generation gas turbine with a power shaft (a) and a single spool power generation gas turbine with a reheat stage and two combustion chambers (b)

is added to insure a stoichiometric combustion. It expands in the multi-stage turbine that produces the major portion of power. As seen in the following sections, the implementation of the reheat process substantially increases the thermal efficiency of gas turbines. The underlying thermodynamic principles of this concept is the reheat process, which has been very well known in steam turbine design for more than a century. However, in gas turbine design, adding a second combustion chamber to a conventionally designed gas turbine seemed to be associated with unforeseeable problems. Based on design experiences with *Compressed Air Energy Storage* (CAES) gas turbines with two combustion chambers, *Brown Boveri* designed and successfully manufactured the first series of power generation gas turbines with a reheat stage and two combustion chambers.

18.1.1 Gas Turbine Process

Accurate prediction of thermal efficiency of a gas turbine engine requires the knowledge of the compressor, combustion chamber, and turbine efficiencies as well as the bearing losses and the losses in auxiliary systems. Furthermore, detailed knowledge of the amount of mass flows with their extraction and injection pressures for cooling the turbine blades and the rotor discs are necessary. In addition, a detailed gas table that accounts for thermodynamic properties of humid air as well as the properties of the combustion gas must be implemented into the calculation procedure. Assuming air and combustion gas as calorically perfect gases results in significant errors. Figure 18.6 exhibits a schematic diagram that shows in detail the extraction of different cooling mass flows and their injection locations.

Mass flow through P1 extracted from plenum 3 cools the rotor and does not participate in power generation; mass flows through P2 and P3 cool the second and first turbine stages and remain in the system; and finally, mass flow through P4

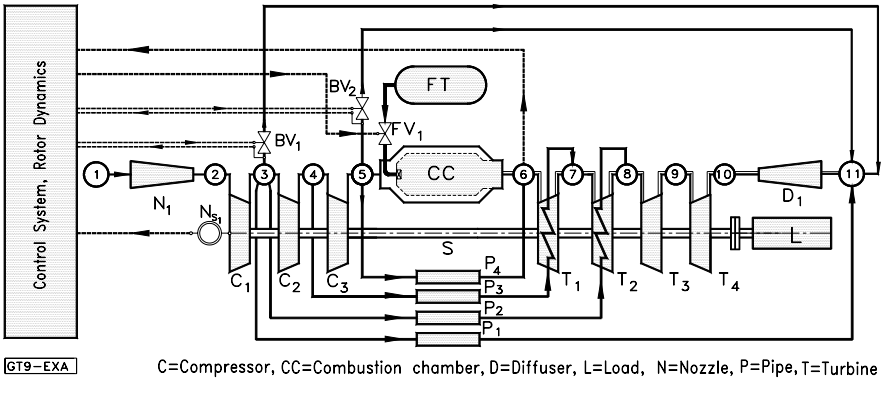

Fig. 18.6: Schematic of a single spool gas turbine illustrating the mass flow extraction from compressor for different cooling purposes

reduces the combustion chamber exit temperature before it enters the turbine. At stations 6, 7, 8, and 11 humid air is mixed with combustion gas resulting in a local change of water/air and fuel/air ratios, therefore changing the entire thermodynamic properties including the special gas constant *R*. In the absence of the above information, reasonable assumptions relative to component efficiencies can be made to qualitatively determine the thermal efficiency and its tendency with regard to parameter variation. In the following section, a simple thermal efficiency calculation procedure is derived that is appropriate for varying different parameters and qualitatively determining their impacts on thermal efficiency.

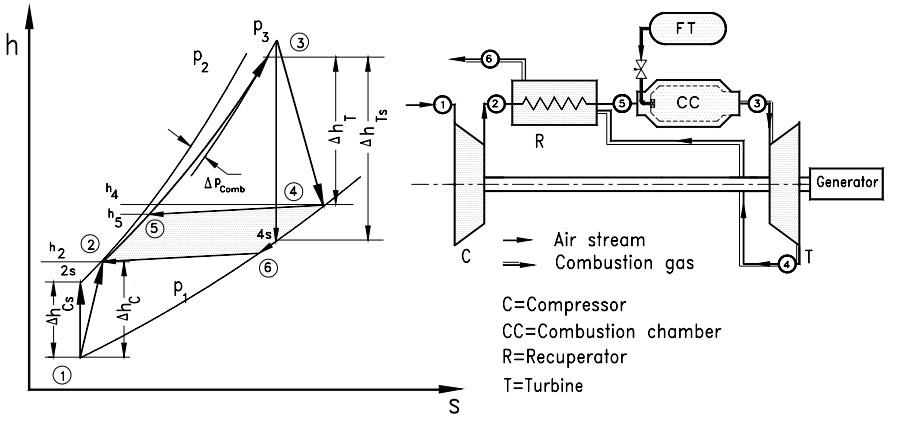

Fig. 18.7: Simple sketch of a gas turbine with recuperator

The gas turbine with its corresponding process is sketched in Fig. 18.7. It consists of a compressor, a recuperator, a combustion chamber and a turbine. Exhaust gas from the turbine is diverted into the recuperator heating up the compressed air before entering the combustion chamber. The individual processes are compression, expansion, fuel addition and combustion, and heat exchange in recuperator. The compressor and turbine enthalpy differences are calculated from:

$$\begin{aligned} h_2 - h_1 &= \frac{h_{2s} - h_1}{\eta_c} \\ h_3 - h_4 &= \left(h_3 - h_{4s}\right) \eta_T \end{aligned} \tag{18.1}$$

We introduce the following definitions for the recuperator air- and gas-side (*RA, RG)*, as well as combustion chamber (*CC)* pressure loss coefficients:

$$\begin{aligned}
\zeta_{RA} &= \frac{\Delta P_{RA}}{P_2}, \quad \text{with} \quad \Delta P_{RA} = P_2 - P_5 \\
\zeta_{RG} &= \frac{\Delta P_{RG}}{P_1}, \quad \text{with} \quad \Delta P_{RG} = P_4 - P_6 \\
\zeta_{CC} &= \frac{\Delta P_{CC}}{P_2}, \quad \text{with} \quad \Delta P_{CC} = P_5 - P_3
\end{aligned} \tag{18.2}$$

The thermal efficiency is defined as:

$$\eta_{in} = \frac{L_{net}}{\dot{Q}_{in}} = \frac{L_T - L_C}{\dot{Q}_{in}} = \frac{\dot{m}_T l_T - \dot{m}_C l_C}{\dot{Q}_{in}} \tag{18.3}$$

The specific net power is calculated from:

$$\frac{L_{net}}{\dot{m}_1} = \frac{L_T - L_c}{\dot{m}_1} = \frac{\dot{m}_3 l_T - \dot{m}_1 l_C}{\dot{m}_1} = (1+\beta)\, l_T - l_c \tag{18.4}$$

with the fuel air ratio $\beta = \dot{m}_f / \dot{m}_1$. Replacing the specific turbine power l_T by the enthalpy difference from Eq. (18.1), we find:

$$\begin{aligned}
\frac{\dot{m}_3}{\dot{m}_1} l_T &= (1+\beta)\left(h_3 - h_4\right) = \eta_T (1+\beta)\left(h_3 - h_{4s}\right) \\
\frac{\dot{m}_3}{\dot{m}_1} l_T &= \eta_T (1+\beta) \bar{c}_{PT}\left(T_3 - T_{4s}\right) \\
\frac{\dot{m}_3}{\dot{m}_1} l_T &= \eta_T (1+\beta)\, \bar{c}_{PT}\, T_3 \left(1 - \frac{T_{4s}}{T_3}\right)
\end{aligned} \tag{18.5}$$

Equation (18.5) expresses the isentropic enthalpy difference in terms of a product of averaged specific heat at constant pressure and the isentropic temperature difference. The specific heat in Eq.(18.5) exhibits an averaged value between the two given temperatures:

$$\bar{c}_{PT} = \frac{h_3 - h_{4s}}{T_3 - T_{4s}} \tag{18.6}$$

The temperature ratio in Eq. (18.5) can be related to the pressure ratio as follows:

$$\frac{T_3}{T_{4s}} = \left(\frac{p_3}{p_4}\right)^{\left(\frac{k-1}{k}\right)_T} = \pi_T^{\left(\frac{k-1}{k}\right)_T} = \pi_T^{m_T}, \quad \text{with } m_T \equiv \left(\frac{k-1}{k}\right)_T \tag{18.7}$$

with Eq. (18.7), Eq. (18.5) becomes:

$$\frac{\dot{m}_3}{\dot{m}_1} l_T = \eta_T (1+\beta) \bar{c}_{PT} T_3 \left(1 - \pi_T^{-m_T}\right) \tag{18.8}$$

Because of the pressure losses across the combustion chamber, the turbine and compressor pressure ratios are not the same ($\pi_T \neq \pi c$). Implementing the pressure losses of the combustion chamber and recuperator air side, we find:

$$\pi_T = \frac{p_3}{p_4} = \frac{p_2 - \Delta p_{RA} - \Delta p_{cc}}{p_1 + \Delta p_{RA}} = \frac{p_2}{p_1}\left(\frac{1 - \zeta_{RA} - \zeta_{cc}}{1 + \zeta_{RA}}\right) = \pi_c \frac{1 - \zeta_{RA} - \zeta_{cc}}{1 + \zeta_{RA}} \tag{18.9}$$

We set the fraction on the right hand side of Eq. (18.9):

$$\varepsilon = \frac{1 - \zeta_{RA} - \zeta_{cc}}{1 + \zeta_{RA}} \tag{18.10}$$

and arrive at:

$$\pi_T = \varepsilon \pi_c, \text{for } \varepsilon = 0,\ \zeta_{RA} = \zeta_{CC} = \zeta_{RA} = 0 \quad \text{and for } \varepsilon < 0\ \ \zeta_{RA} \neq 0,\ \zeta_{cc} \neq 0 \tag{18.11}$$

For parameter variation, following values may be used: $\zeta_{RA} \cong \zeta_{RG} \cong 2-5\%$, $\zeta_{cc} \cong 3-5\%$. Following exactly the same procedure defined by Eqs. (18.4) through (18.11), we find the compressor specific work as:

$$l_C = \frac{1}{\eta_C} \bar{c}_{Pc} T_1 \left(\pi_C^{m_C} - 1\right), \text{ with } m_C = \left(\frac{k-1}{k}\right)_C \tag{18.12}$$

Inserting Eqs. (18.8) and (18.12) into Eq. (18.4), we arrive at:

$$\eta_{th} = \frac{\eta_T \bar{c}_{PT} \frac{T_3}{T_1}\left[1 - (\varepsilon \pi_c)^{-m_T}\right](1+\beta) - \frac{1}{\eta_c} \bar{c}_{Pc}\left(\pi_c^{m_c} - 1\right)}{\bar{c}_{Pcc}\left[(1+\beta)\frac{T_3}{T_1} - \frac{T_5}{T_1}\right]} \tag{18.13}$$

The turbine inlet temperature T_3, the environmental temperature T_1, and thus their ratio T_3/T_1 is considered as a known parameter. This parameter can also be used for parametric studies. Therefore it is desirable to express the ratio T_5/T_1 in terms of T_3/T_1. We find this ratio by utilizing the recuperator effectiveness η_R:

$$\eta_R = \frac{h_5 - h_2}{h_4 - h_2} \cong \frac{T_5 - T_2}{T_4 - T_2} \tag{18.14}$$

From compressor and turbine energy balance, Eq. (18.1) we find

$$\begin{aligned} T_2 &= T_1 + (T_{2s} - T_1)\frac{1}{\eta_c} = T_1 + T_1\left(\pi_c^{m_c} - 1\right)\frac{1}{\eta_c} \\ T_4 &= T_3 - (T_3 - T_{4s})\eta_T = T_3 - T_3\left[1 - (\varepsilon\pi_c)^{-m_T}\right]\eta_T \end{aligned} \tag{18.15}$$

Equation (18.15) in dimensionless form yields:

$$\begin{aligned} \frac{T_2}{T_1} &= 1 + \frac{1}{\eta_c}\left(\pi_c^{m_c} - 1\right) \\ \frac{T_4}{T_1} &= \frac{T_3}{T_1} - \frac{T_3}{T_1}\eta_T\left[1 - (\varepsilon\pi_c)^{-m_T}\right] \end{aligned} \tag{18.16}$$

Introducing the temperature ratio $\theta = T_3/T_1$, the temperature ratio T_4/T_1 Eq. (18.16) becomes:

$$\frac{T_4}{T_1} = \Theta\left\{1 - \left[1 - (\varepsilon\pi_c)^{-m_T}\right]\eta_T\right\} \tag{18.17}$$

To determine the temperature ratio T_5/T_1, we re-arrange Eq. (18.14)

$$\frac{T_5}{T_1} = \eta_R\left(\frac{T_4}{T_1} - \frac{T_2}{T_1}\right) + \frac{T_2}{T_1} \tag{18.18}$$

Using Eqs. (18.16) and (18.17), Eq. (18.18) is re-arranged as

$$\frac{T_5}{T_1} = \eta_R\left[\theta\left\{1 - \left[1 - (\varepsilon\pi_c)^{-m_T}\right]\eta_T\right\} - 1 - \frac{1}{\eta_c}\left(\pi_c^{m_c} - 1\right)\right] + 1 + \frac{1}{\eta_c}\left(\pi_c^{m_c} - 1\right) \tag{18.19}$$

Introduce Eqs. (18.19) and the definition $\theta = T_3/T_1$ into Eq. (18.13), the thermal efficiency equation for a gas turbine with a recuperator is written as:

$$\eta_{th} = \frac{\bar{c}_{PT}\eta_T\theta\left[1-(\varepsilon\pi_c)^{-m_T}\right](1+\beta) - \frac{1}{\eta_c}\bar{c}_{Pc}\left(\pi_c^{m_c}-1\right)}{\bar{c}_{PCC}\left\{\theta\left(1+\beta-\eta_R\right) - \left[1+\frac{1}{\eta_c}\left(\pi_c^{m_c}-1\right)\right]\left[1-\eta_R\right] + \theta\eta_R\eta_T\left[1-(\varepsilon\pi_c)^{-m_T}\right]\right\}} \tag{18.20}$$

From Eq. (18.20) special cases are obtained. Setting $\eta_R = 0$ gives the thermal efficiency of a gas turbine without recuperator. The ideal case of Brayton cycle is obtained by setting all loss coefficients equal to zero, all efficiencies equal to unity, and $\bar{c}_{PC} = \bar{c}_{PCC} = \bar{c}_{PT} = const.$ Equation (18.20) properly reflects the effects of individual parameters on the thermal efficiency and can be used for preliminary parameter studies. As an example, Fig. 18.8 shows the effect of pressure ratio, the turbine inlet temperature, and the component efficiency on thermal efficiency for two different cases. As Fig. 18.8 shows, for each turbine inlet temperature, there is one optimum pressure ratio. For temperature ratios up to $\theta = 3.5$ pronounced efficiency maxima are visible within a limited π-range. Approaching higher inlet temperature, however, this range widens significantly.

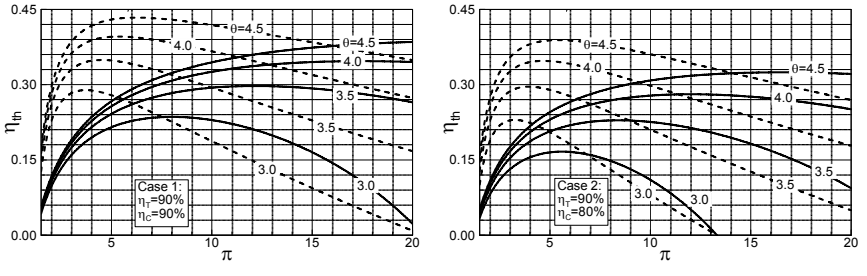

Fig. 18.8: Thermal efficiency as function of pressure ratio with turbine inlet temperature ratio as parameter for (a) gas turbine with recuperator, dashed curves and (b) without recuperator, solid curves. $\eta_R = 0.75$, $\zeta_{CC} = 0.05$, $\zeta_{RA} = \zeta_{RG} = 0.03$, for Case 1 and Case 2. In Case 2 the turbine efficiency is lowered from 90% to 80%.

For a gas turbine without recuperator, the thermal (efficiency solid curves in Fig. 18.8) shows that for $\theta = 4.0$, increasing the pressure ratio above 15 does not bring any noticeable efficiency increase. However, it requires the compressor to have one or two more stages. The temperature ratio $\theta = 4.0$ corresponds to a turbine inlet temperature of $T_3 = 1{,}200K$ at a compressor inlet temperature of $T_1 = 300.0K$.

Figure 18.8, dashed curves indicate that tangibly higher thermal efficiencies at a substantially lower pressure ratio can be achieved by utilizing recuperators. This is particularly advantageous for small gas turbines (so called "micro-turbines") with power ranging from 50 to 200 kW. The required low maximum pressure ratio can easily be achieved by a single-stage centrifugal compressor. Comparing Case1 and Case 2 in Fig. 18.8 shows that thermal efficiency reduces if low efficiency components are applied.

18.1.2 Improvement of Gas Turbine Thermal Efficiency

The above parameter study indicates that for a conventional gas turbine with a near-optimum pressure ratio with or without the recuperator, the turbine inlet temperature is the parameter that determines the level of thermal efficiency. For small size gas turbines recuperator is an inherent component of the gas turbine. For large power generation gas turbines, however, it is not a practical option. Using a recuperator in a large gas turbine requires significantly lower pressure ratio that results in a large volume recuperator and turbine. As a result in order to improve the thermal efficiency of conventional gas turbines, increasing the turbine inlet temperature seems to be the only option left. Considering this fact, in the last three decades, gas turbine manufacturer have been concentrating their efforts to introduce more sophisticated cooling technologies that is essential for increasing the turbine inlet temperature of conventional gas turbines.

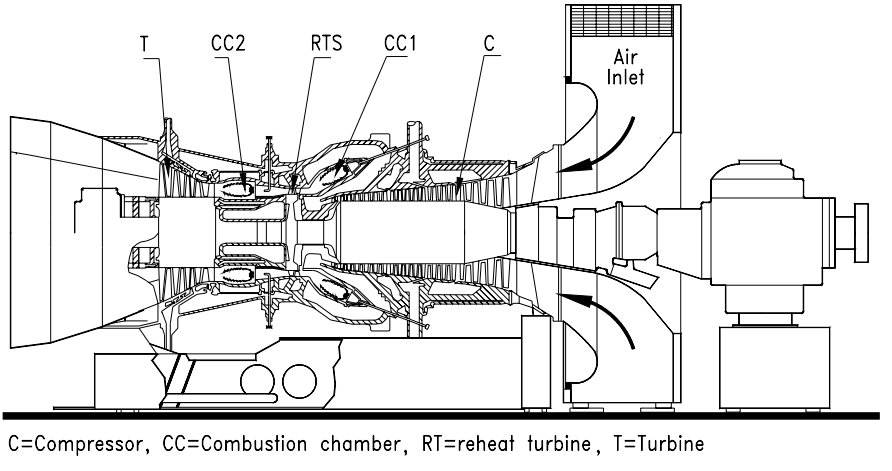

Fig. 18.9: A schematic cross section of GT-24 gas turbine engine with a single stage reheat turbine and a second combustion chamber

To substantially improve the thermal efficiency without a significant increase in turbine inlet temperature, a well known reheat principle as a classical method for thermal efficiency augmentation is applied. Although this standard efficiency improvement method is routinely applied in steam turbine power generation, it did not find its way into the aircraft and the power generation gas turbine design. The reason was the inherent problem of integrating a second combustion chamber into a conventionally designed gas turbine engine. This issue raised a number of unforeseeable design integrity and operational reliability concerns. ABB (formerly Brown Boveri & Cie) was the first to develop a gas turbine engine with one reheat stage turbine followed by a second combustion chamber and a multi-stage turbine, Fig. 18.9.

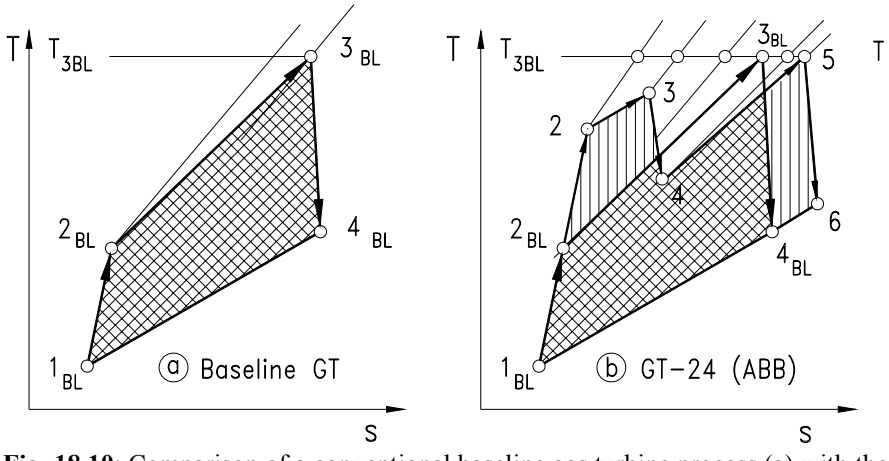

Fig. 18.10: Comparison of a conventional baseline gas turbine process (a) with the GT-24 process (b) from [1]

A comparative study by Schobeiri [1] emulates, among others, two conceptually different power generation gas turbine designs utilizing components, whose detailed aerodynamic performance characteristics were known. The first one is a conventional gas turbine, whereas the second one has a reheat turbine stage and a second combustion chamber resembling GT-24 [2]. Starting from a given environmental condition (pressure, temperature) and a consolidated turbine inlet temperature T_{3BL} = 1200 °C for both engines, Fig 18.10a, the thermal efficiency is determined by the compressor pressure ratio and the compressor and turbine polytropic efficiencies η_c, η_T and is plotted in Figure 18.11a.As curve 1 shows, for the given pressure ratio, which is not identical with the optimum pressure ratio, an efficiency of η_{th} = 35% is calculated. Substantial efficiency improvement is achieved by introducing a single-stage reheat principal as applied to GT-24. Details of the process are sketched in Fig. 18.10b with the baseline process as the reference process. The vertically cross-hatched area in Fig. 18.10b translates into the efficiency improvement, which in the

case of GT-24 resulted in efficiency improvement of 5.5% above the baseline efficiency. A detailed dynamic engine simulation of the GT-24 gas turbine engine with GETRAN© [3] verified a thermal efficiency of $\eta_{th} = 40.5\%$ plotted in Fig. 18.11a, curve 2. This tremendous efficiency improvement was achieved despite the facts that (a) the compressor pressure ratio is much higher than the optimal one for baseline engine and (b) the introduction of a second combustion chamber inherently causes additional total pressure losses. Further calculation showed that introducing a third combustion chamber would result only in a marginal improvement of 1 to 1.5% thermal efficiency, which does not justify the necessary R&D efforts to integrate a third combustion chamber. The specific work comparison is plotted in Fig. 18.11(b), which shows a significant increase in specific work.

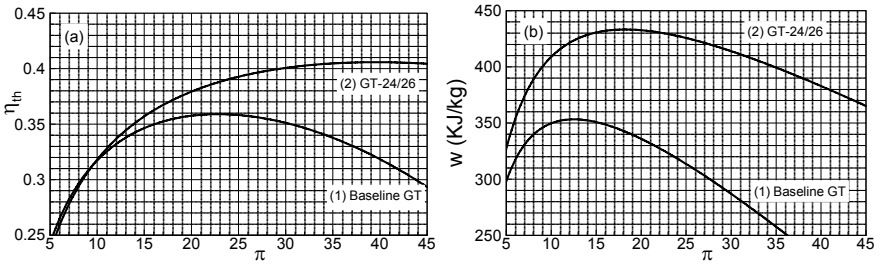

Fig. 18.11: Comparison of efficiency and specific work between a conventional baseline gas turbine and GT-24, (a) efficiency, (b) specific work

Additional efficiency improvement requires a major technology change. As Schobeiri [2] showed, major improvement can be achieved by using the UHEGT-technology (ultra high efficiency gas turbine technology). This technology eliminates the combustion chambers altogether and places the combustion process inside the stator and rotor blade passages (see section 18.6).

18.2 Non-linear Gas Turbine Dynamic Simulation

The continuous improvement of efficiency and performance of aircraft and power generation gas turbine systems during the past decades has led to engine designs that are subject to extreme load conditions. Despite the enormous progress in the development of materials, at the design point, the engine components operate near their aerodynamic, thermal, and mechanical stress limits. Under these circumstances, any adverse dynamic operation causes excessive aerodynamic, thermal, and subsequent mechanical stresses that may affect the engine safety and reliability, and, thus, the operability of the engine if adequate precautionary actions are not taken.

Considering these facts, an accurate prediction of the above stresses and their cause is critical at the early stages of design and development of the engine and its components. This section focuses on simulation of dynamic behavior of gas turbine

engines and their components. The simulation spectrum encompasses single- and multi-spool gas turbine engines, turbofan engines, and power generation gas turbine engines. The simulation concept is based on a generic modularly structured system configurations. In the last six chapters, the gas turbine components were represented by individual modules described mathematically by systems of differential equations. Based on these and other necessary modules, a generic concept is presented that provides the reader with necessary tools for developing computer codes for simulation of arbitrary engine and plant configurations ranging from single-spool thrust generation to multi-spool thrust/power generation engines under adverse dynamic operating conditions. It can easily be extended to rocket engines, combined cycles, co-generation cycles and steam power plants. A multi-level system simulation treats different degrees of complexity ranging from global adiabatic simulation to detailed diabatic one. The dynamic behavior of the subject engine is calculated by solving a number of systems of partial differential equations which describe the unsteady behavior of the individual components. Accurate prediction of the dynamic behavior of the engine and the identification of critical parameters by the method enables the engine designer to take appropriate steps using sophisticated control systems. The method may also be used to proof the design concept of the new generation of high performance engines. The modular structure of the concept enables the user to independently develop new components and integrate them into the simulation code. As representative examples, four different case studies are presented that deal with dynamic simulation of a compressed air energy storage gas turbine, different transient cases with single- and multi-spool thrust and power generation engines were simulated. The transient cases range from operating with a prescribed fuel schedule, to extreme load changes and generator shut down.

18.2.1 State of Dynamic Simulation, Background

Dynamic behavior of aircraft gas turbine engines was investigated earlier by several researchers using the component performance map representation for simulating engines. Seldner et al. [4] and Koenig and Fishbach [5] utilized overall component performance maps in their simulation program GENENG, which performs purely steady-state computations. In order to account for system dynamics, Seller and Daniele [6] extended the above code by introducing simplified dynamic equations. In a report about a hybrid simulation of single- and twin-spool turbofan engines, Szuch [7] described the representation of engine components by overall performance maps. To estimate gas turbine starting characteristics, Agrawal and Yunis [8] generated a set of steady component characteristics, where the turbine and compressor components are represented by overall steady performance maps. The engine representation by performance maps, as briefly addressed above and comprehensively discussed by Schobeiri [3], exhibits a useful tool for approximating engine behavior within the operation range defined by the component maps. However, the detailed information that is crucial for engine development and design cannot be provided at this simulation level. Furthermore, the above representation is not viable for providing

the control system designer with the necessary input parameters, such as those describing the aero-thermodynamic and structural conditions of the compressor and turbine blade rows. Consequently, the response of the real system to the intervention of the controller cannot be verified. These and other parameters are required inputs to the controller for triggering precautionary actions such as active surge control, achieved by adjusting variable compressor stator blades.

In order to address the above issues, Schobeiri [9], [10], [11], [12], [13], [14] developed the modularly structured computer code COTRAN for simulating the nonlinear dynamic behavior of single-shaft power generation gas turbine engines. To account for the heat exchange between the material and the working fluid during a transient event, diabatic processes are employed in COTRAN for combustion chamber and recuperator components. The dynamic expansion process through the turbine component is accomplished by a row-by-row calculation using the stage characteristics. COTRAN reflects real engine configurations and components, and is routinely used at the early stages of design and development of new gas turbine engines. Dynamic simulations of different single-shaft engines performed with COTRAN were reported by Schobeiri and Haselbacher [15]. Although COTRAN represents an advanced, nonlinear dynamic code, its simulation capability is limited to single-shaft power generation gas turbine engines and, thus, cannot be used for simulating multi-spool aircraft engines. Considering this circumstance, Schobeiri and his co-workers [3], [16], [17] developed a new computational method with the corresponding, generic, modularly structured computer code GETRAN for simulating the nonlinear dynamic behavior of single- and multi-spool high pressure core engines, turbofan engines, and power generation gas turbine engines. The code is capable of simulating aircraft engines having up to five spools with variable geometry, with or without additional power generation shafts.

18.3 Engine Components, Modular Concept, Module Identification

A schematic component arrangement and modeling of a twin-spool core engine is shown in Fig.18.12. The corresponding modules are implemented into the engine modular configuration schematic Fig.18.13. Figures 18.14 and 18.15 display the lists of components with their corresponding modular representations and symbols that are described by the method presented in Chapters 14 through 19. They exhibit the basic components essential for generically configuring any possible aero- and power generation gas turbine engines. These modules are connected with each other with a plenum, which is a coupling component between two or more successive components. As briefly explained in Chapters 14, the primary function of the plenum is to couple the dynamic information of entering and exiting components such as mass flow, total pressure, total temperature, fuel/air ratio, and water/air ratio. After entering the plenum a mixing process takes place, where the aforementioned quantities reach their equilibrium values. These values are the same for all outlet components.

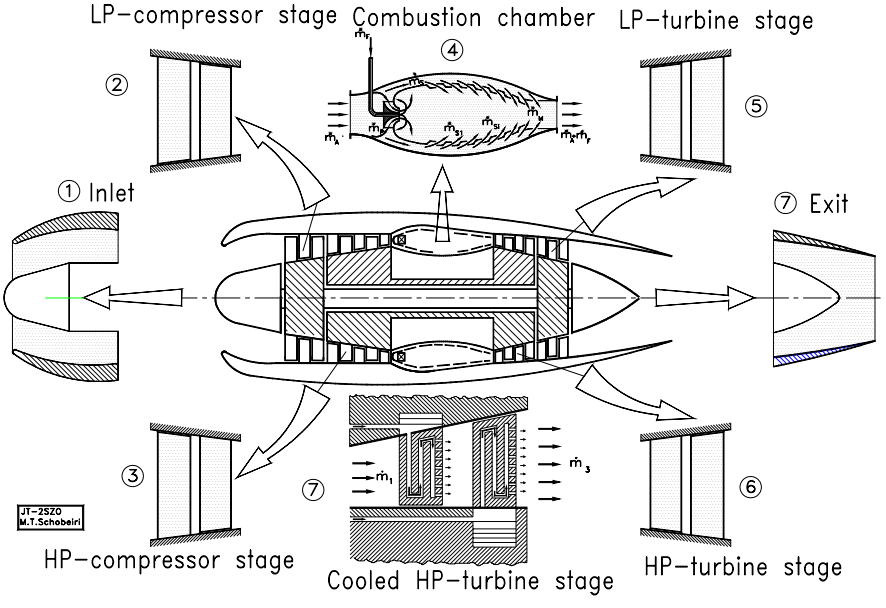

Fig. 18.12: Schematic of a twin spool core engine, component decomposition

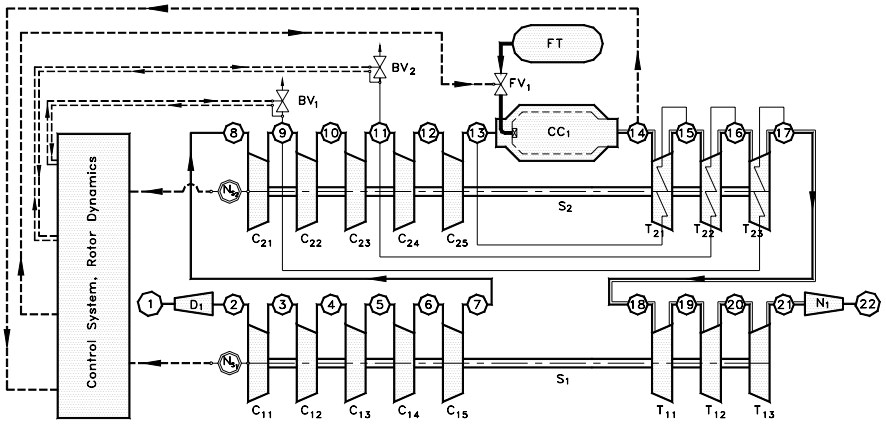

Fig. 18.13: Modular configuration of engine exhibited in Fig.18.12

A survey of power and thrust generation gas turbine engines has led to the practical conclusion that any arbitrary aircraft or power generation gas turbine engine and its derivatives, regardless of configuration, i.e., number of spools and components, can be generically simulated by arranging the components according to the engine configuration of interest. The present nonlinear dynamic method is based on this generic, modularly structured concept that simulates the transient behavior of existing and new engines and their derivatives. The modules are identified by their names, shaft number, and inlet and outlet plena. This information is vital for automatically generating the system of differential equations representing individual modules. Modules are then combined into a complete system which corresponds to the engine configuration. Each module is physically described by the conservation laws of thermo-fluid mechanics which result in a system of nonlinear, partial differential or algebraic equations. Since an engine consists of a number of components, its modular arrangement leads to a system containing a number of sets of equations. The above concept can be systematically applied to any aircraft or power generation gas turbine engine.

The general application of the modular concept is illustrated in Figs. 18.12 and 18.13. The twin-spool engine shown in Fig. 18.12 exemplifies the modular extension of the single-spool base engine. It consists of two spools with the shaft S_1 and S_2, on which the low and high pressure components such as compressors and turbines are assembled. The two shafts are coupled by the working media air and combustion gas. They rotate with different speeds which are transferred to the control system by the sensors N_{s1} and N_{s2}. Air enters the inlet diffuser D_1, which is connected with the multi-stage compressor assembled on S_1, and is decomposed in several compressor stages C_{1i}. The first index, 1, refers to the spool number and the second index, i, marks the number of the compressor stage. After compression in the S_1 compressor stage group, the air enters the second compressor (HP- compressor) assembled on the S_2 shaft that consists of stages C_{21}-C_{25}. In the combustion chamber (CC_1) high temperature combustion gas is produced by adding the fuel from the tank FT. The gas expands in the high pressure turbine that consists of stages T_{21} - T_{23}. By exiting from the last stage of HP-turbine, the combustion gas enters the low pressure turbine consisting of stages T_{11} - T_{13} and is expanded through the exit nozzle. Two bypass valves, BV_1 and BV_2, are connected with the compressor stator blades for surge prevention. The fuel valve, FV_1, is placed between the fuel tank, FT, and the combustion chamber, CC_1. The pipes, P_i, serve for cooling air transport from the compressor to cooled turbines. The compressor stage pressures, the turbine inlet temperature, and the rotor speed are the input signals to the control system, which controls the valve cross sections and the fuel mass flow.

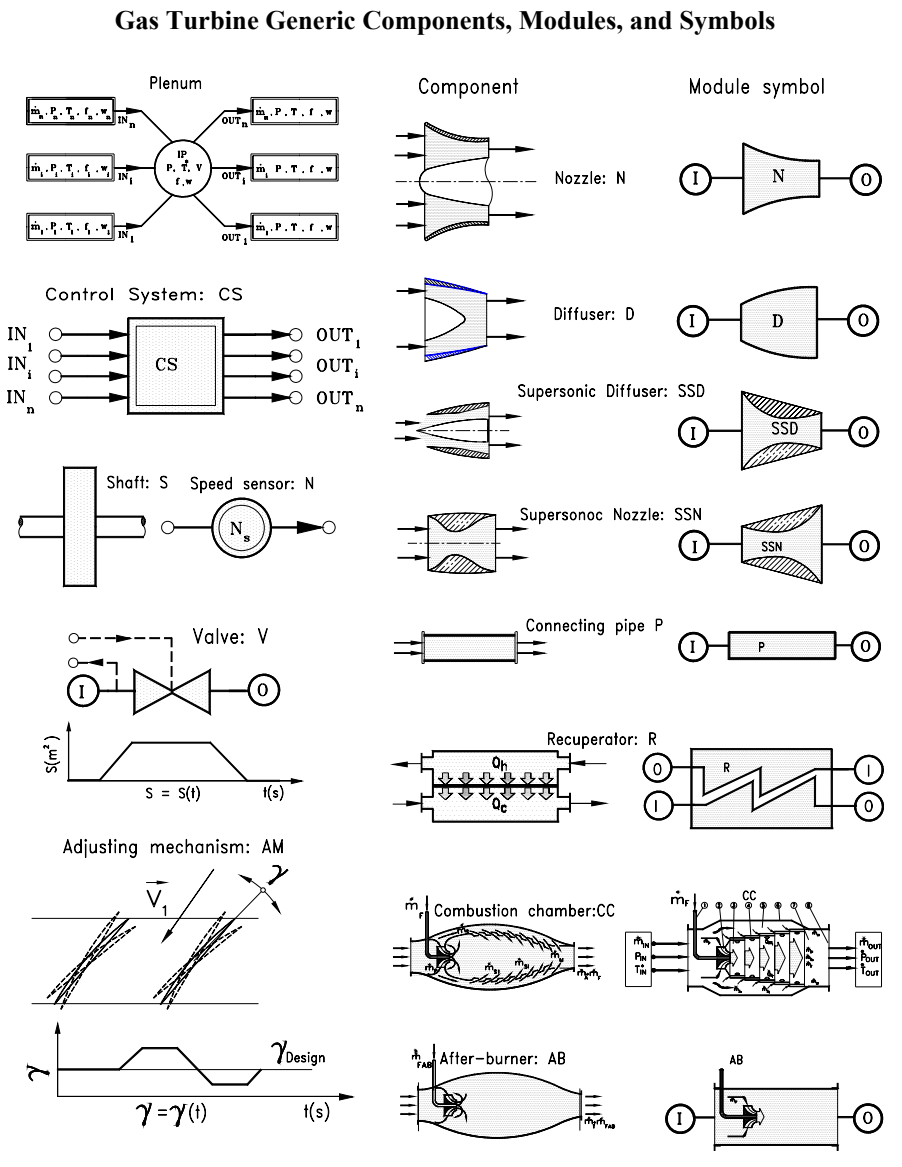

Fig. 18.14: Components, modules, and their symbols: Plenum, Control system CS, Shaft S, with moment of inertia I and the rotational velocity ω, Speed sensor N, Valve with an arbitrary ramp for closing and opening the cross section S, Adjusting mechanism AM for stator blade adjustment, Subsonic nozzle N, Subsonic diffuser D, Supersonic Diffuser SSD, Supersonic nozzle SSN, Recuperator R, Combustion Chamber CC, and Afterburner AB

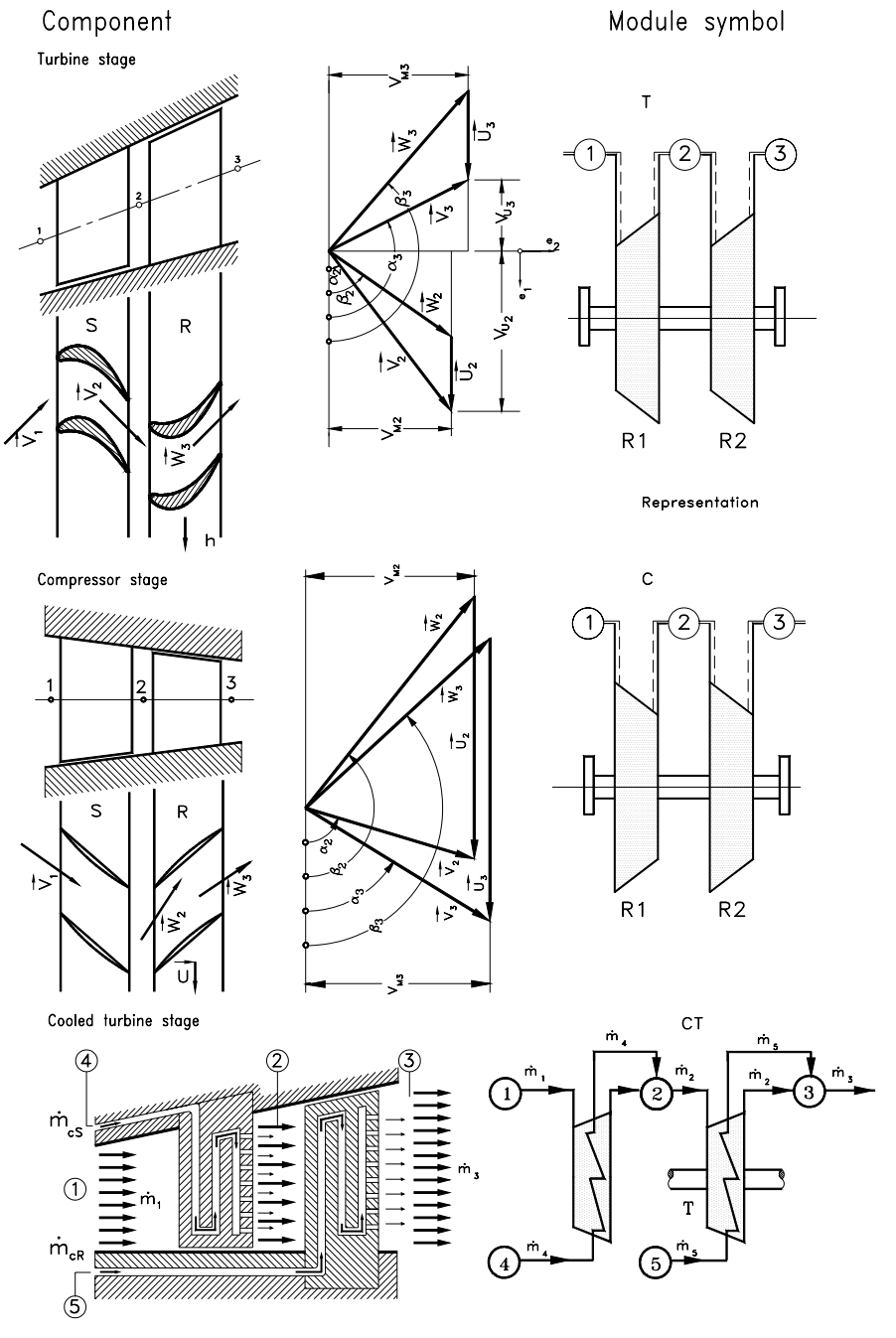

Fig. 18.15: Adiabatic turbine stage with the module T, adiabatic compressor stage with the module C, cooled turbine stage with the module CT

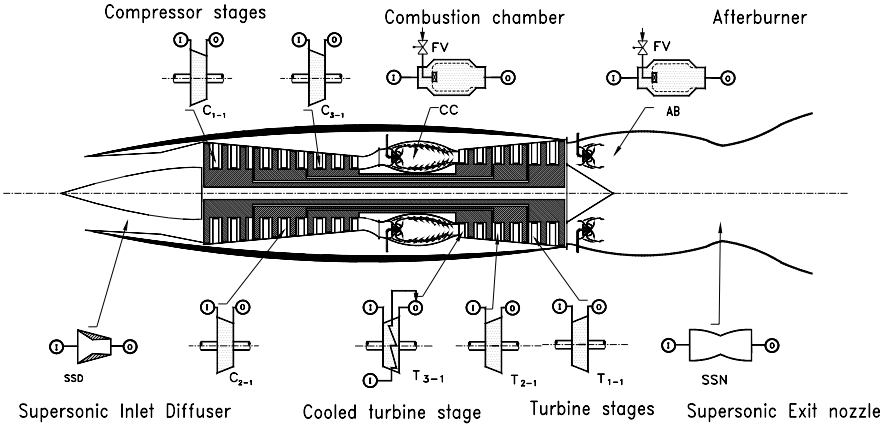

Fig. 18.16: Schematic of a 3-spool high performance core engine, component decomposition

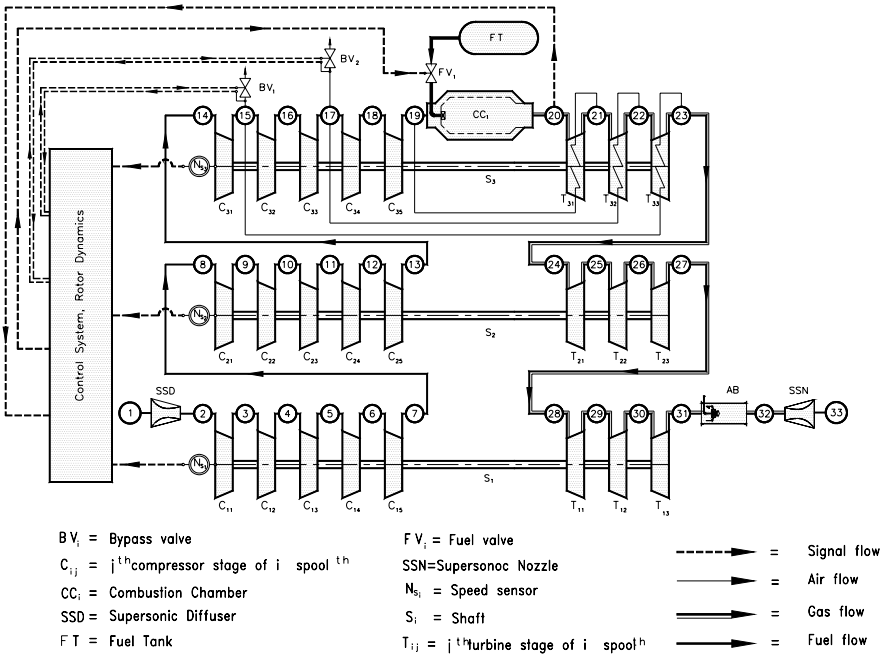

Fig. 18.17: Modular configuration of the 3-spool engine shown in Fig. 18.16. The three compressors and turbines are connected aerodynamically. The plena addressing, the spool number, and the component number uniquely identify the set of differential equations that describe the module.

Figure 18.16 shows a more complex example of a three-spool supersonic engine with its modular decomposition. Figure 18.17 exhibits a systematic modular configuration of Fig. 18.16 that is represented by a large system of differential and algebraic equations.

18.4 Levels of Gas Turbine Engine Simulations, Cross Coupling

Accuracy of gas turbine dynamic simulation is determined by the level of component modeling. It increases by increasing the level of simulation complexity. Four levels of simulation are introduced:

Zeroth Simulation Level: Is applied to simple cases such as those in [4] through [7], utilizing a fixed system configuration with steady state component characteristics that are described by algebraic equations, simplified differential equations, and lookup tables and maps. Furthermore, there is no dynamic coupling between the components. Since this simulation level does not account for engine dynamics, it will not be discussed further.

First Simulation Level: This level uses component global performance map only for turbines and compressors. The maps are generated using the row-by-row adiabatic calculation method detailed in Chapters 18 and 19. The other components such as recuperators, coolers, combustion chambers, pipes, nozzles, and diffusers are simulated according to methods discussed in Chapters 14 through 17. Primary air, secondary combustion gas, and metal temperature of the combustion chamber are calculated. All modules are coupled with plena insuring a dynamic information transfer to all modules involved. Modules are described by algebraic and differential equations.

Second Simulation Level: This level utilizes adiabatic row-by-row or stage-by-stage calculation for compressor and turbine modules. For combustion chamber, primary air, secondary combustion gas, and metal temperature are calculated. Dynamic calculations are performed throughout the simulation, where the modules are coupled by plena. Each module is described by differential and algebraic equations.

Third Simulation Level: This level uses diabatic row-by-row calculation for compressor and turbine modules. This level delivers a very detailed diabatic information about the compressor and turbine component dynamic behavior. It utilizes cooled turbine and compressor stages and simultaneously calculates the blade temperatures. For combustion chamber, primary air, secondary combustion gas, and metal temperature are calculated. Dynamic calculations are performed throughout the simulation, whereas the modules are coupled by plena. Each module is described by differential and algebraic equations. The details of information delivered by this level and degree of complexity is demonstrated by the following example. The first two stages of a four-stage turbine component of high performance gas turbine engine must

be cooled. For the first four turbine rows we use the diabatic expansion process that requires three differential equations for describing the primary flow, three differential equations for describing the cooling flow, and one differential equation for describing the blade temperature. This leads from two cooled turbine stages to 28 differential equations.

The generic structure allows to cross-couple level 1 to 3. For example, we wish to simulate a gas turbine engine with a global compressor performance map, but need to obtain detailed information about turbine blade temperature, which is necessary to calculate the relative expansion between the blades and the casing, then we may use the diabatic calculation method. In this case, we cross-couple the first and third level simulation.

18.5 Non-linear Dynamic Simulation Case Studies

Three different case studies dealing with three completely different gas turbine systems are presented. Table 18.1 shows the matrix of the cases where the engine types and transient-type simulations are listed. These studies demonstrate the capability of the generic structured method we discussed in Chapters 15 through 18 to dynamically simulate complex systems with high accuracy.

Table 18.1: Simulation Case Studies

TESTS	GAS TURBINE TYPE	TRANSIENT TYPE
CASE 1	CAES: Compressed air energy storage power generation gas turbine engine, zero-spool, single shaft, two turbines, two combustion chambers	Generator trip, emergency shut down.
CASE 2	Single-spool, single-shaft, power generation gas turbine engine, BBC-GT9	Adverse load changes.
CASE 3	Three-Spool, four-shaft, thrust and power generation core engine	Operation with fuel schedule.

The case studies presented in this chapter are related to the real world engine simulation and are intended to provide the reader with an insight into the non-linear engine dynamic simulation. The selected cases ranging from zero-spool, single shaft power generation to three-spool four shaft thrust and power generation gas turbine engines provide detailed information about the engine behavior during design and off-

design dynamic operation. For each engine configuration the simulation provides aero-thermodynamic details of each individual component and its interaction with the other system components. Since the presentation of the complete simulation results of the three cases listed in Table 1 would exceed the frame of this chapter, only a few selected plots will be displayed and discussed for each case.

18.5.1 Case Study 1: Compressed Air Energy Storage Gas Turbine

The subject of this case study is a zero-spool, single-shaft compressed air energy storage (CAES) gas turbine[18], which is utilized to efficiently cover the peak electric energy demand during the day. Continuous increase of fuel costs has motivated the power generation industry to invest in technologies that result in fuel saving. Successful introduction of combined cycle gas turbines (CCGT) has drastically improved the thermal efficiency of steam power plants that is equivalent to a significant fuel saving. Further saving is achieved by using the excess electrical energy available during the period of low electric energy demand (6-8 hours during the night) to compress air into a large storage. During the peak demand, the compressed air is injected into the combustion chambers and is mixed with the fuel. After the ignition process is completed, the high pressure, high temperature gas expands in the turbine generating electric energy for about 2 to 4 hours. In contrast to a CCGT, the period of operation of a CAES plant is restricted to a few hours per day resulting in a daily startup followed by a shutdown procedure. This relatively high frequency of startups and shutdowns may cause structural damages resulting in reduced life time if the startup and shutdown procedures are not performed properly. The condition for a safe startup procedure is outlined in this study that helps the engine and control system designer to integrate into their design procedure. The CAES gas turbine system, Fig. 18.18, with the simulation schematic shown in Fig. 18.19 features a large volume plenum (8) for storing the compressed air, a high-pressure combustion chamber (HPCC), a high-pressure turbine (HPT), a low-pressure combustion chamber (LPCC), a low-pressure turbine (LPT2), a cold-air pre-heater with a low pressure and high pressure side (LPP and HPP-side) and a generator (G). During the steady-state turbine operation, cold air from the air-storage facility, plenum 8, passes through the shutdown valve (V_1) to the inlet plenum (1), where it is divided into combustion and cooling-air flows. The addition of fuel in HPCC causes the combustion air to be heated up to the combustion chamber's exit temperature. Immediately upstream of HPT, the combustor mass flow mixed with a portion of the cooling-air flow, which has already been preheated in HPP. As a result, the gas temperature of the turbine mass flow lies below the combustion chamber's exit temperature. After expansion in HPT, the combustion chamber (LPCC) mass flow is mixed in LPT inlet plenum (4) with the rest of the preheated cooling-air flow and the sealing-air flow. After expansion in LPT, the gas gives off some of its heat in LPP before leaving the gas turbine system.

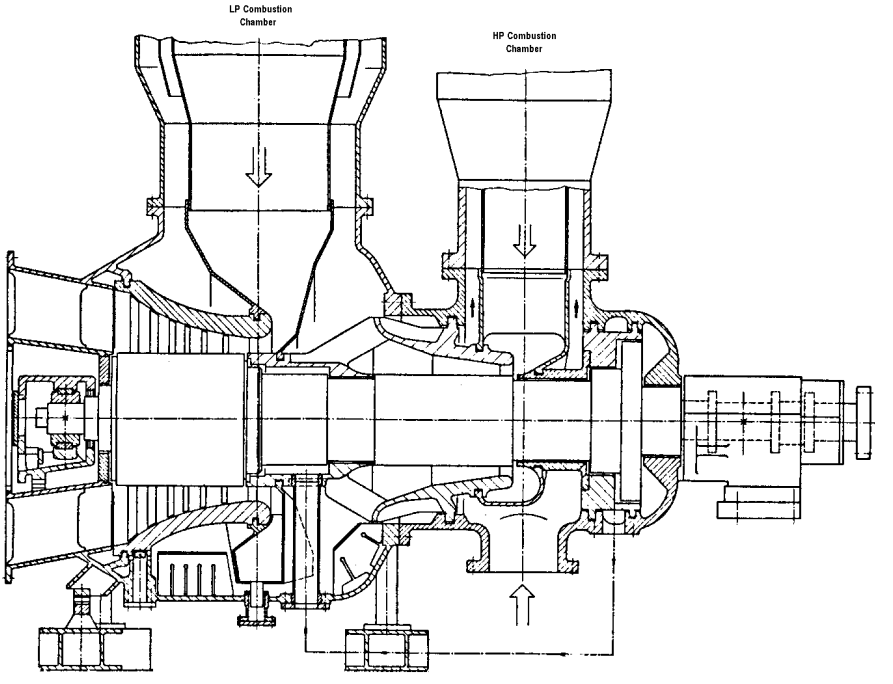

Fig. 18.18: BBC-CAES-Huntdorf gas turbine engine [18]

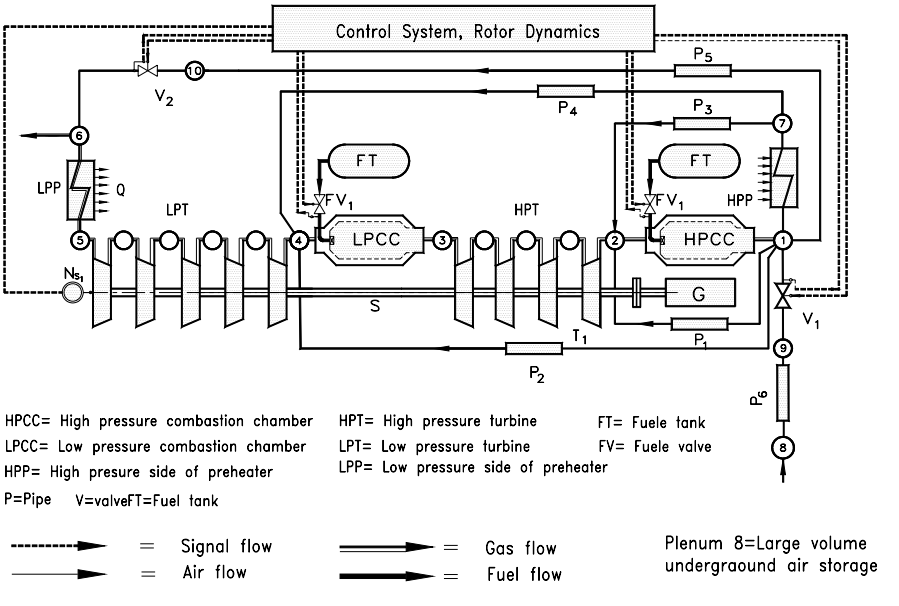

Fig. 18.19: Simulation schematic of the CAES shown in Fig. 18.18

Figure 18.19 shows how the various components are interconnected. Plenum 8, the air storage facility, is connected via two identical pipes (P6) to two shutdown valves (V_1). During steady-state operation, the blow-off valve (V_2) remains closed, being opened in the event of a disturbance likely to cause rapid shutdown. In such an event, the valve blows off some of the gas, thereby limiting the maximum rotor speed. For the sake of clarity, the pre-heater (P) has been separated into its air and gas sides, designated HPP and LPP, respectively.

18.5.1.1 Simulation of Emergency Shutdown: Starting from a steady operating point, a generator trip with rapid shutdown was simulated assuming a failure of the control system. This circumstance necessitates an intervention by the hydraulic emergency system. This incident simulates an extreme transient process within some of the components, as explained briefly. After the generator trip, the rotor is strongly accelerated because of full turbine power acting on it, Fig. 18.20(a).

The hydraulic emergency system intervenes only when the speed corresponding to the hydraulic emergency overspeed trip is reached. This intervention involves

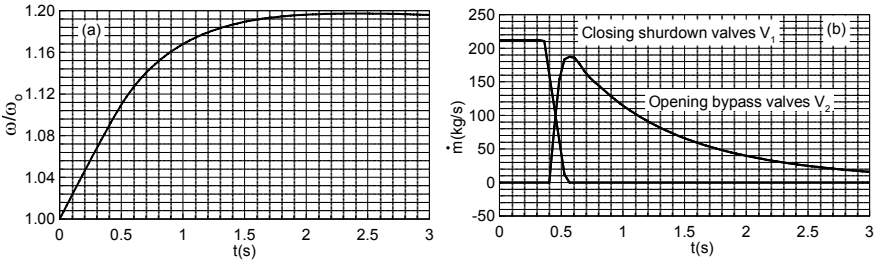

Fig. 18.20: Relative angular velocity (a) and mass flows (b) as function of time. The Inlet-shutdown valves V_1 remain open until the trip speed at t= 0.35 s has been reached. The same procedure is true for opening the blow-off valves V_2. Closing the shutdown valves follow the ramp shown in Fig. 18.20(b).

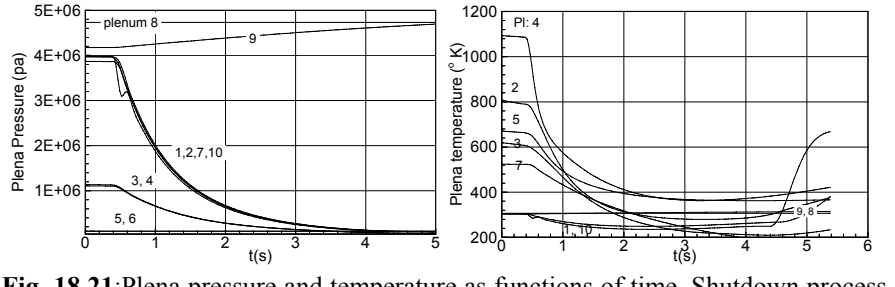

Fig. 18.21:Plena pressure and temperature as functions of time. Shutdown process causes rapid depressurization in high pressure plena1, 2, 7, and 10.

closing the fuel valves, FV_1 and FV_2, and air valves, V_1, after which the system no longer receives any energy from outside, Fig. 18.20(b). It also involves opening the bypass/blow-off valve V_2 that allows the high pressure air contained in both large volume combustion chambers as well as in the HP-side of pre-heater to discharge. The closing process of the inlet and shutdown valves and the opening of the bypass valves are shown in Fig. 18.20(b). This process results in a steady drop in plena pressures and temperatures. As Fig. 18.21 shows, the pressure drop in the high-pressure section is initially steeper than in the low-pressure section. This means that the enthalpy difference of the high-pressure turbine is reduced more rapidly than that of the low-pressure turbine. Immediately after the blow-off valve is opened, an abrupt pressure drop takes place in plenum 10, which is connected to plenum 1 via pipe P5. Thereafter, dynamic pressure equalization takes place between the two plena. This drop in pressure and temperature causes a corresponding drop in the shaft power and the mass flow throughout the engine.

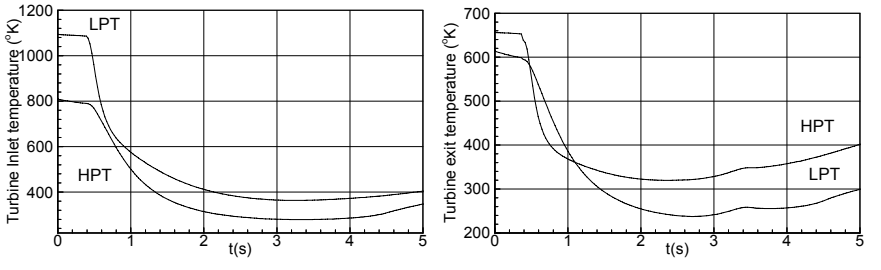

Fig. 18.22: Turbine inlet and exit temperature as functions of time. Note changes of the exit temperature at t=3.4 s

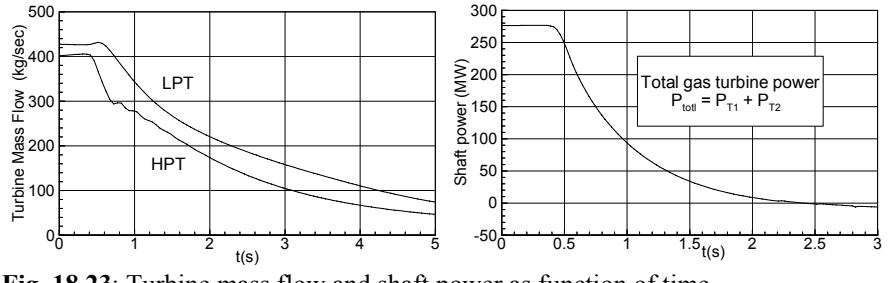

Fig. 18.23: Turbine mass flow and shaft power as function of time

Figure 22.22 shows the resulting drop in turbine inlet and exit temperature. The continuous decrease in turbine mass flow causes a strong dissipation of shaft power resulting in the excessive increase of turbine exit temperature. In order to avoid thermal damages to blades, a small stream of cold air is injected into the turbine flow path that causes a reduction in temperature gradient. This is shown in Fig. 18.22 for the exit temperature at t = 3.4 s.

Dynamic behavior of the rotor speed is generally determined by the turbine power acting on the rotor. How the rotor behaves in response to a generator trip depends, in particular, on how long the full turbine power is available, a process monitored by the control and safety monitoring system. When the control system functions normally, trip is signaled without delay to the shutdown valve. Failure of the control system causes the hydraulic emergency system to intervene. The intervention begins only when the speed corresponding to the hydraulic emergency overspeed trip is reached. During this process, and also the subsequent valve dead time, the rotor receives the full turbine power. The closing phase is characterized by a steady reduction in energy input from outside, which finally becomes zero. The total energy of the gases still contained in the system is converted by the two turbines into mechanical energy, causing the rotor speed to increase steadily, Fig. 18.20. When the instantaneous turbine power is just capable of balancing the friction and ventilation losses, the rotor speed reaches its maximum, after which it begins to decrease. Reducing the turbine mass flow, Fig. 18.23 (left), below the minimum value discussed in Chapter 19, causes the shaft power to dissipate completely as heat resulting in negative values as Fig. 18.23 (right) shows. From this point on, the rotational speed starts to decrease. The figure depicts the mass flow through both turbines as representatives for the entire engine as well as the total shaft power.

18.5.2 Case Study 2: Power Generation Gas Turbine Engine

The subject of this case study is the dynamic simulation of a BBC-GT9 gas turbine which is a single-spool single shaft power generation gas turbine engine. It is utilized as a stand-alone power generator or in conjunction with combined cycle power generation. The engine shown in Fig. 18.24 consists mainly of three compressor stage groups, a combustion chamber, a turbine, a control system, and a generator. The simulation schematic of this engine is presented in Fig. 18.25. The rotor speed and turbine inlet temperature are the input parameters for the controller, its output parameters are the fuel mass flow (fuel valve opening), and the mass flows of the bypass valves (bypass valve opening). The dynamic behavior of BBC-GT9 was experimentally determined for transient tests with extreme changes in its load. Its transient data was accurately documented by Schobeiri [3]. Starting from a given network load schedule, the dynamic behavior of the gas turbine is predicted and the results are presented.

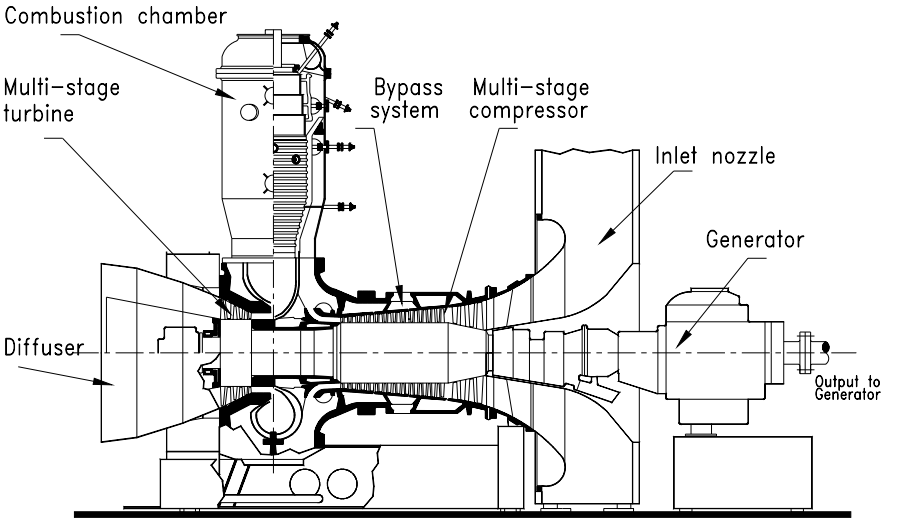

Fig. 18.24: A single spool power generation gas turbine, BBC-GT9

The engine under consideration consists mainly of three compressor stage groups, a combustion chamber, a turbine, a control system, and a generator. The simulation schematic of this engine is shown in Fig. 18.25. For dynamic simulation, the first, second and third stage groups are simulated in row-by-row fashion. A similar row-by-row calculation procedure is applied to the turbine component. The rotor speed and the turbine inlet temperature are the input parameters for the controller, its output parameters are the fuel mass flow (fuel valve opening), and the mass flows of the bypass valves (bypass valve opening).

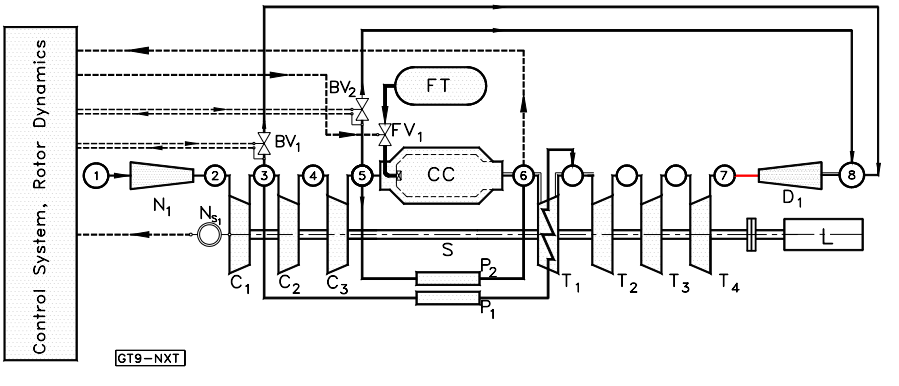

Fig. 18.25: Simulation schematic of BBC-GT9 shown in Fig. 18.24

Simulation of an Adverse Dynamic Operation: Starting from steady state, in accordance with the load schedule indicated in Fig. 18.26 (left), curve 1, after one second, a generator loss of load is simulated that lasts for six seconds. The rotor at first reacts with a corresponding increase in rotational speed, Fig. 18.26 (right), which results in a rapid closing of the fuel valve, Fig. 18.31 (right). The rotational speed is then brought to an idling point and held approximately constant. The process of control intervention lasts until a constant idling speed is attained. After that, there is an addition of load in sudden increases, such that the gas turbine is supplying approximately 25% of its rated load, Fig. 18.26. The rotor first reacts to this addition of load with a sharp decrease in rotational speed, as exhibited in Fig. 18.26, causing a quick opening of the fuel valve, Fig. 18.31. After completion of the transient process, the steady off-design state is reached.

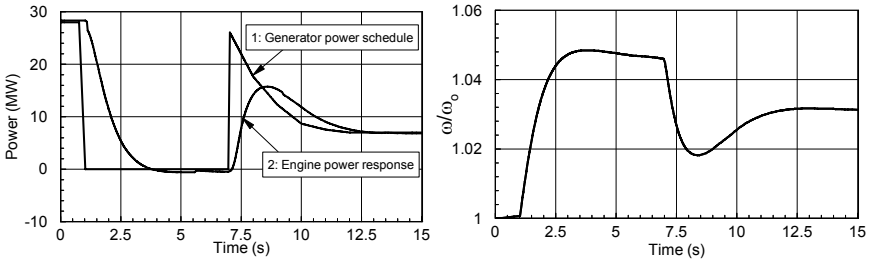

Fig. 18.26: Left, generator load schedule curve 1, sequence of events: Steady operation from 0 to 1 second, sudden loss of load, idle operation, sudden addition of load, continuous decrease of load to 25%. Curve 2: engine power response. Right, relative shaft speed as a function of time.

Plena Pressure and Temperature Transients: The above adverse dynamic operation has triggered temporal changes of flow quantities within individual components. Figure 18.27 shows how the plena pressure and temperature change with time.

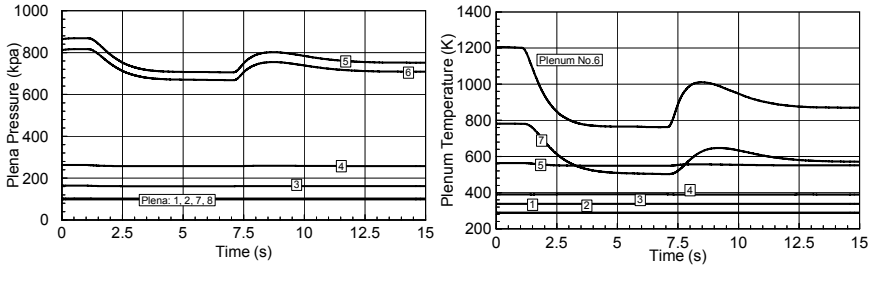

Fig. 18.27: Plena pressure and temperature as functions of time. Individual plena are labeled.

Decrease of turbine power and increase of the shaft speed, Fig. 18.26, has caused the HP-compressor exit pressure in plenum 5 to decrease. Temperature at combustion chamber exit, plenum 6, and turbine exit, plenum 7, follow the course of fuel injection shown in Fig. 18.31(right). The plena temperature upstream of the combustion chamber are not affected.

Compressor and Combustion Chamber Mass Flow Transients: Figure 18.28 exhibits the mass flow transients through LP-, IP-, and HP-compressors. While IP- and HP-stage groups have the same mass flow, the LP-part has a greater mass flow. The difference of 1 kg/s is due to the cooling mass flow extraction. As briefly mentioned, the increase in shaft speed and the simultaneous decrease in compressor power consumption leading to compressor pressure drop has caused an increase in compressor mass flow during the process of loss of load that lasts up to t = 6 sec.

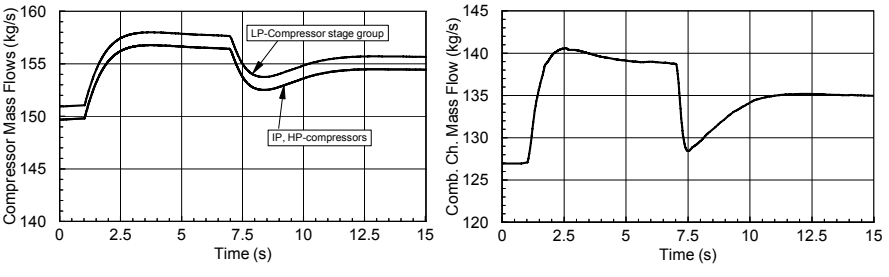

Fig. 18.28: Compressor and combustion chamber mass flows as functions of time

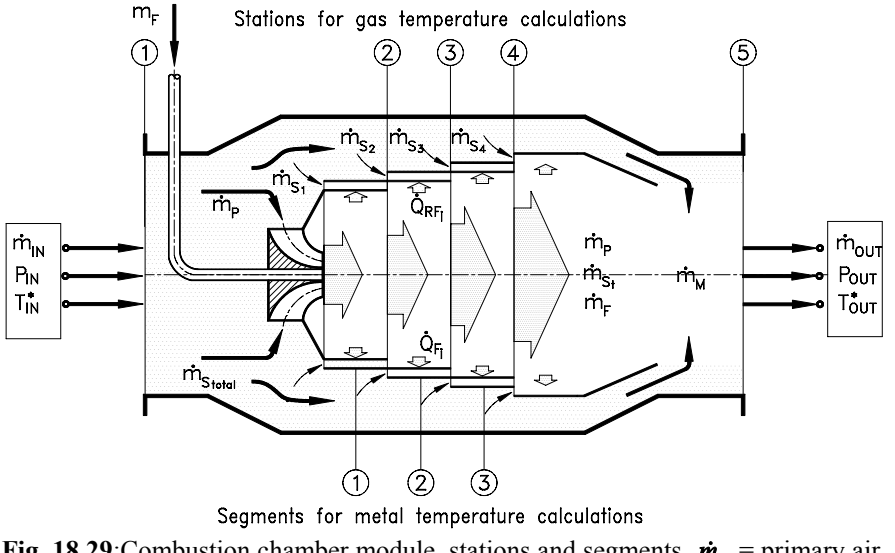

Fig. 18.29:Combustion chamber module, stations and segments, $\dot{m}_P$ = primary air, $\dot{m}_{Stot}$= total secondary air, $\dot{m}_{Si}$= individual secondary air

The sudden load addition reduces the compressor mass flow. The combustion chamber mass flow shows a similar course with a substantial difference. A substantial portion of compressor mass flow is extracted for combustion chamber exit temperature mixing cooling.

Combustion Chamber Gas and Metal Temperature Transients: The combustion chamber component used in this simulation has three segments that separate the primary combustion zone from the secondary cooling air zone. Its module is shown in Fig. 18.29. Figure 18.31 exhibits the combustion chamber gas and metal temperatures as functions of time. Compressed air enters the combustion chamber at station 1, Figs. 18. 29, and 18.31. Fuel is added and the segment cooling occurs according to the procedure described in Chapter 17. The secondary mass flow portions $\dot{m}_{Si}$ serve as cooling jets and are mixed with the combustion gas, thus reducing the gas temperature. Before exiting, the combustion gas is mixed with the mixing air stream $\dot{m}_M$, further reducing the temperature. Figure 18.31 (right) shows the mean segment temperatures. In accordance with the measurements on this gas turbine, the flame length extends from station 1 to 3, which makes the segment number 2 the hottest one. We assumed that all secondary cooling channels are open.

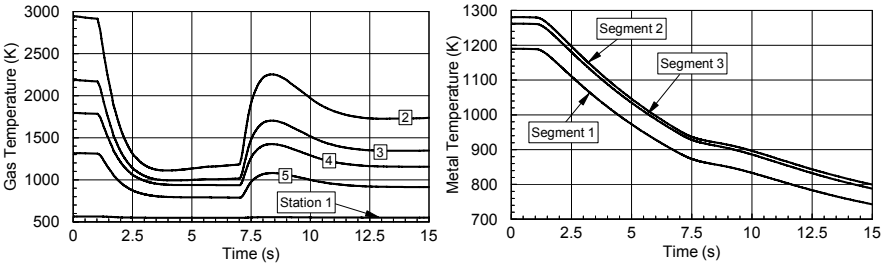

Fig. 18.30: Combustion chamber gas and metal temperature at different positions as functions of time

Turbine and Fuel Mass Flow Transients: Figure 18.31 (left) exhibits the turbine mass flow transient, which is dictated by the compressor dynamic operation. Difference between the turbine and the compressor mass flow is the injected fuel mass flow. The particular course of fuel mass flow shown in Fig. 18.31 (right) is due to the intervention of the control system. An increase in rotational speed causes the controller to close the fuel valve. Subsequent addition of generator load results in a steep drop of rotational speed which causes an opening of the fuel valve.

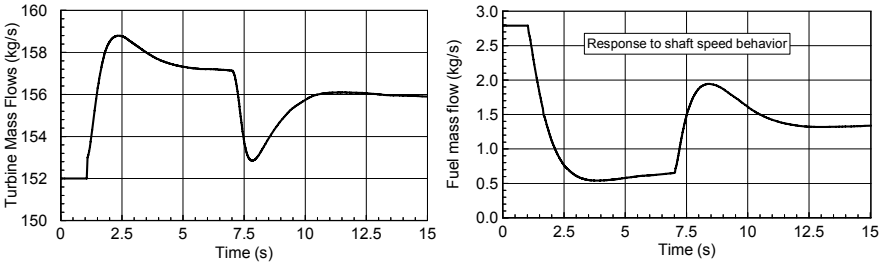

Fig. 18.31: Turbine and fuel mass flow as functions of time. The fuel mass flow is controlled by the shaft rotational speed.

18.5.3 Case Study 3: Simulation of a Multi-spool Gas Turbine Engine

The subject of this study is the non-linear dynamic simulation of a gas turbine engine with a higher degree of complexity than the previous cases. For this purpose a three-spool thrust generating gas turbine engine is designed that incorporates advanced components. The three-spool four shaft high performance gas turbine engine consists of a low pressure spool that incorporates the LP-compressor and turbine connected via shaft S_1. The intermediate pressure spool integrates the IP-compressor and turbine connected via shaft S_2. The high pressure spool carries the HP-compressor and HP-turbine on shaft S_3. To increase the level of engine complexity, a fourth shaft, S_4, with

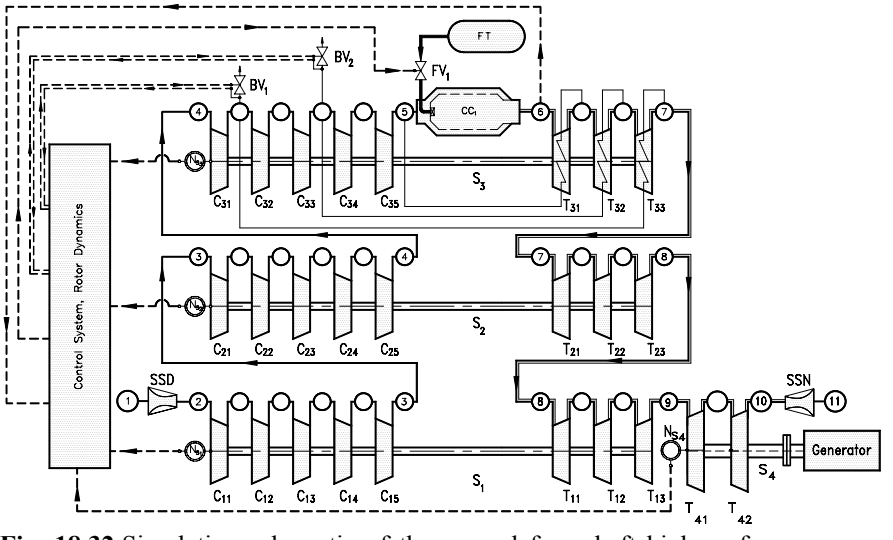

Fig. 18.32:Simulation schematic of three-spool four shaft high performance gas turbine engine. Spool 1 incorporates LP-compressor and LP-turbine connected via shaft S_1; Spool 2 incorporates IP-compressor and IP-turbine connected via shaft S_2; Spool 3 incorporates HP-compressor and HP-turbine connected via shaft S_3.

the power generating turbine, T_4, was attached to the exit of the three-spool gas generating unit as shown in Fig. 18.32. The transient operation is controlled by a given fuel schedule. The component nomenclature for this configuration is the same as for the previous cases. The simulation schematics shown in Fig. 18.32 represents the modular configuration of the gas turbine.

Fuel Schedule, Rotor Response: The dynamic behavior of the above engine is simulated for an adverse acceleration-deceleration procedure. The transient operation is controlled by an open loop fuel schedule shown in Fig. 18.33 (left). The three-spools and the fourth shaft run independently at different rotational speed, Fig. 18.33 (right).

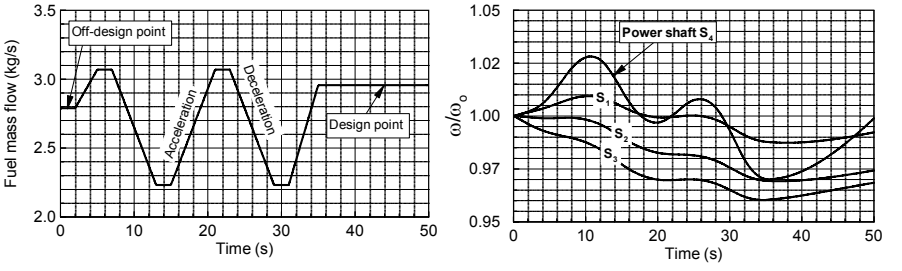

Fig. 18.33: Fuel schedule (left) starts with an off-design mass flow followed by a cyclic acceleration-deceleration procedure. Rotational speed of the three spools and the power shaft.(right).

The fuel schedule generated fully arbitrarily simulates an acceleration-deceleration procedure with emphasis on deceleration. We start with the steady-state operation and reduce the fuel mass flow to $\dot{m}_F = 2.8 kg/s$ for about two seconds. During this short period of time, the engine operates in a dynamic state which is followed by a cyclic acceleration-deceleration event with the ramps given in Fig. 18.33. The dynamic operation triggers a sequence of transient events within individual components that are discussed in the following sections.

Rotor Speed Behavior: The transient behavior of the three spools as well as the power shaft is determined by the net power acting on the corresponding rotor. For each individual spool, the cyclic acceleration-deceleration event has caused a dynamic mismatch between the required compressor power consumption and the turbine power generation as shown in Fig. 18.34. While LP- and IP-spools 2 and 3 decelerate under the influence of negative net power, the HP-spool 3 reacts faster to the acceleration. Since the fuel schedule places special weight upon deceleration, the rotational speeds of all three spools have a decelerating tendency as shown in Fig. 18.34.

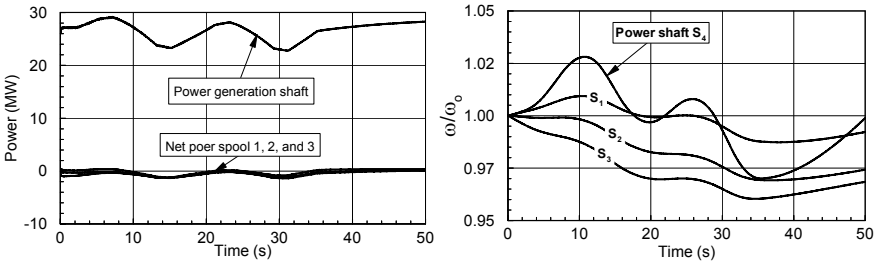

Fig. 18.34: Net power acting on the three spools causing a dynamic mismatch; power generated by the fourth shaft (left). Relative rotor speed of three spools and the fourth shaft.

Pressure and Temperature Transients within Plena: The change in fuel mass flow triggers a chain of transient events within the plena as shown in Fig. 18.35.

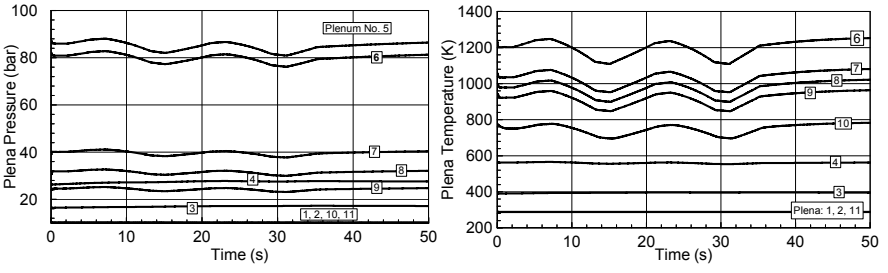

Fig. 18.35: Plena pressure (left) and temperature (right) as functions of time

Plena pressure 5 and 6 which corresponds to the exit pressure of the HP-compressor and the combustion chamber, are strongly affected by the cyclic fuel change, whereas the other plena that correspond to the inlet and exit plena of the remaining components experiences moderate changes. The plena temperature distributions downstream of the combustion chamber shown in Fig. 18.35 (right) reflect the course of the fuel schedule.

Combustion Chamber Gas and Metal Temperature Transients: Figure 18.36 exhibits the combustion chamber gas and metal temperatures as functions of time. The combustion chamber component used in this simulation has three segments that separate the primary combustion zone from the secondary cooling air zone. Its module is shown in Fig. 18.32. Compressed air enters the combustion chamber at station 1, Figs. 18. 36 (left). Fuel is added and the segment's cooling occurs according to the procedure described in Chapter 17. The secondary mass flow portions $\dot{m}_{Si}$ serve as cooling jets and are mixed with the combustion gas, thus reducing the gas temperature. Before exiting, the combustion gas is mixed with the mixing air stream $\dot{m}_M$ further reducing the temperature. Figure 18.36 (right) shows the mean segment

temperatures. The flame length extends from station 1 to 3, which makes the segment number 2 the hottest one. As seen, the gas temperature at station 2 follows the sharp changes in the fuel schedule. By convecting downstream, these sharp changes are smoothed out. Wall temperatures shown in Fig. 18.36 (right) exhibit similar tendencies.

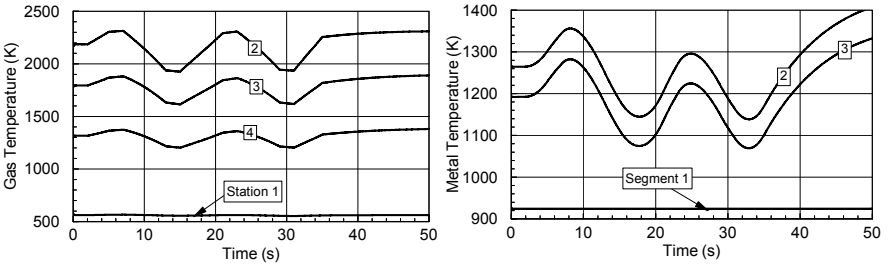

Fig. 18.36: Combustion chamber gas and metal temperature as functions of time

Compressor and Turbine Mass Flow Transients: Figure 18.37 (left) exhibits the compressor mass flow transients, which are dictated by the compressor dynamic operation. The difference in compressor mass flow is due to the mass flow extraction for cooling purposes. Turbine mass flows are illustrated in Fig. 18.37 (right). Except for a minor time lag, they show identical distributions. The difference in turbine and compressor mass flow is due to the addition of fuel.

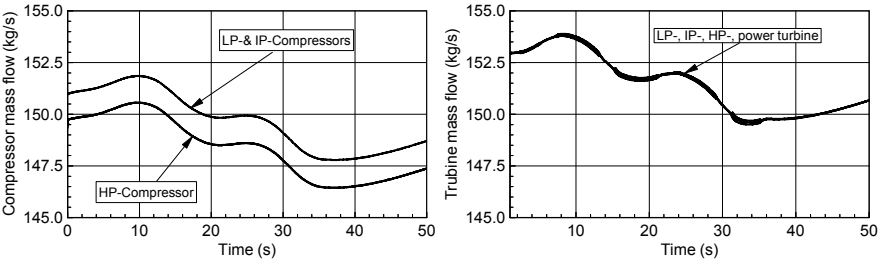

Fig. 18.37: Compressor and turbine mass flow as functions of time

18.6 A Byproduct of Dynamic Simulation: Detailed Efficiency Calculation

One of the interesting aspects of a dynamic simulation is the capability to dynamically calculate the gas turbine thermal efficiency during steady state and dynamic operations. Such calculations are performed to compare the thermal efficiencies of four gas turbines with different design methodologies. The calculations are performed with the nonlinear dynamic code GETRAN. The first gas turbine dynamically simulated for efficiency calculation is a conventional single-shaft, single-combustion

chamber power generation gas turbine. The second one is the ABB, GT 24/26. The third is an ultra-high efficiency gas turbine (UHEGT) with a pre-combustor, a reheat turbine stage and an integrated stator internal combustion as illustrated in Fig. 18.38. For the fourth gas turbine, the combustion process is placed entirely within the stator rows, thus eliminating the combustion chambers all together, Fig. 18.39. The dynamic efficiency calculation results are presented in Fig. 18.40. To accurately determine the thermal efficiency and specific work of the gas turbines, calculations are performed with **GETRAN**© and the results are presented in Fig. 18.40. To compare the degree of efficiency improvement, the thermal efficiency and specific work of a baseline GT, GT-24, and the three UHEGT gas turbines are included in the figures.

For a UHEGT with three-stator combustion, denoted by the curve UHEGT-0C3S, a thermal efficiency above 45% is calculated. This exhibits an increase of at least 5% above the gas turbine engine GT-24, which is close to 40.5% as Fig. 18.40 (left) shows. Increasing the number of stator internal combustion to 4, curve labeled with UHEGT-0C4S, raises the efficiency above 48%. This is an enormous increase compared to any existing gas turbine engine. In the course of this calculation, the UHEGT technology is applied to a gas turbine engine with a pre-combustion chamber, such as the first one in GT-24, Fig.18.48. Using this combustion chamber with two-stator combustion, the curve labeled with UHEGT-1C2S shows an efficiency of 44%. This is particularly interesting for upgrading the existing gas turbines with UHEGT technology. Figure 18.38 (right) reveals the specific work comparison for the gas turbines discussed above. Compared to GT-24, UHEGT technology has about 20% higher specific work, making these engines very suitable for aircraft, stand-alone, as well as for combined cycle power generation applications.

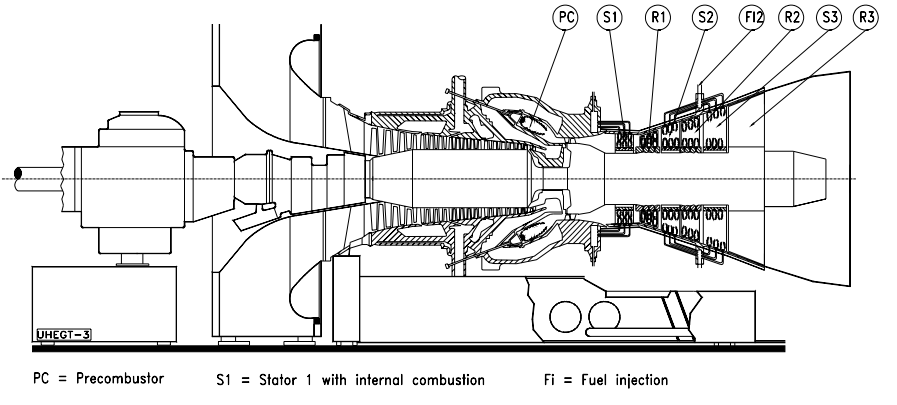

Fig. 18.38: A derivative of the Ultra-High Efficiency Gas Turbine Engine with a multi-stage compressor, a conventional combustion chamber PC, a single-stage reheat turbine RT, a three-stage turbine with an integrated stator internal combustion, B1, B2: compressor bypass blow-off, Fl1, Fl2: Fuel lines to stator. The combustion process takes place inside the pre-combustor and stator flow path, [1].

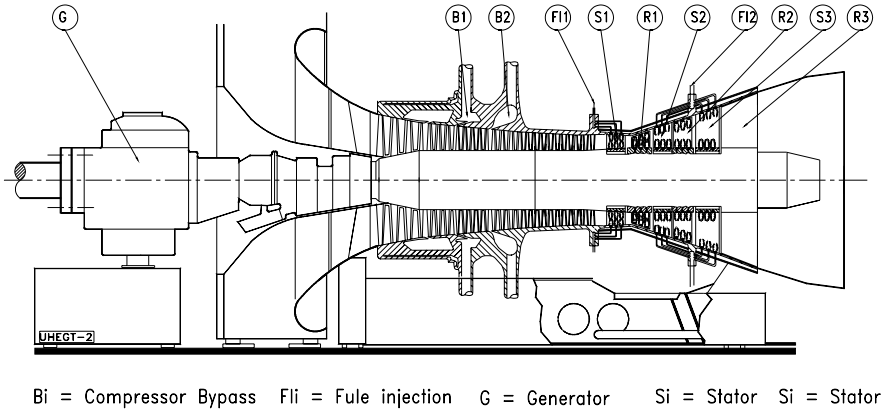

Fig. 18.39: An Ultra-High Efficiency Gas Turbine Engine with a multi-stage compressor, and a three-stage turbine with an integrated stator internal combustion, B1, B2: compressor bypass blow-off, Fl1, Fl2: Fuel lines to stator. The combustion process takes place inside the stator flow path, Schobeiri [1].

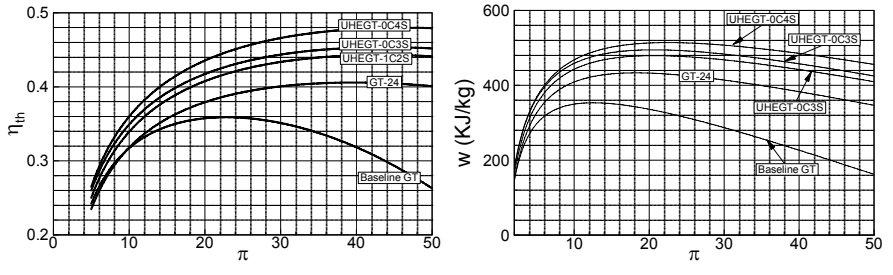

Fig. 18.40: Thermal efficiency (left) and specific work (right) as a function of compressor pressure ratio for the reference baseline gas turbine engine, ABB-GT-24 with two-combustion chamber, the **UHEGT-1C2S** with one conventional combustion chamber and two **UHEGT**-stator combustion, **UHEGT-03S** with three-stator combustion, and **UHEGT-0C4S** with four-stator combustion. Turbine inlet temperature = 1,200^{0}C, calculation with GETRAN [3].

It is interesting to note that this efficiency increase can be established at a compressor pressure ratio of $\Pi_{UHEGT} \approx 35 - 40$, which can be achieved easily by existing compressor design technology with high polytropic efficiency.

In performing the GETRAN© calculation, compressor and turbine efficiencies are calculated on a row-by-row basis. This automatically accounts for an increase of secondary flow losses based on aspect ratio decrease. Thus, in a compressor case, efficiency decrease with pressure ratio increase is inherently accounted for.

18.7 Summary Part III, Further Development

This chapter concludes Part III of the book that started with Chapter 14. The last six chapters dealt with providing the basic non-linear dynamic equations essential for describing the aero-thermodynamic process within individual turbomachinery components from a generic point of view. The four-dimensional time-space equations were simplified and modules were developed based on two-dimensional time-space coordinates. These modules were used to configure simulation schematics of complex gas turbine engines. Four levels of gas turbine engine simulations with cross coupling were presented. Three representative case studies were presented that aimed at better understanding the concept and the necessity for non-linear dynamic simulation.

Improvement of Thermal Efficiency: To introduce the reader to the problematic of gas turbine operation and process, Chapter 18 started with a brief presentation of a simple method for calculating the thermal efficiency of gas turbines, also a few methods for improving the gas turbine process and thermal efficiency were discussed. The parameter study using Eq. (18.20) illustrated the impact of the turbine inlet temperature (TIT) on thermal efficiency. More accurate results are obtained using the dynamic method applied to the corresponding simulation schematics that may incorporate many components and subsystems that are relevant for gas turbine operation. Considering the current advanced state-of-the-art turbine cooling technology and the technologies utilized to protect the blades from excessive thermal stresses by using thermal barrier coatings, there is not much room left for increasing the TIT. Likewise, the development of turbine and compressor components has reached a high level of polytropic efficiency (above 94%) that additional marginal improvement would not significantly improve the thermal efficiency. However, substantially higher thermal efficiencies at a consolidated TIT level can be obtained by taking advantage of the basic thermodynamic principles as demonstrated by the performance evaluation of GT-24/26. Further efficiency improvement can be achieved by utilizing the UHEGT concept for future generation of gas turbine engines. This concept is based on sound thermodynamic principles and offers a substantial improvement, however it requires substantial R&D efforts.

Necessity for Dynamic Simulation: The case studies showed the capability of a generic modularly structured simulation tool based on equations presented beginning in Chapter 14 through 18. From today's computational point of view, simulating a complex gas turbine power plant or an aircraft engine consisting of various components and subsystems that are described by a large number of systems of differential and algebraic equations, does not exhibit any computational obstacle. It is well known that problems with new gas turbine types arise during dynamic operation. Many of these problems can be eliminated in the early stage of design and development by dynamically simulating possible adverse scenarios that may lead to component and system failures.

Modeling Enhancement: As explained, the modular concept is based on a two-dimensional time space approximation. The models described in Part 3 can be

extended to fully four-dimensional time space models. Using the unsteady Navier-Stokes equations requires considerable computational effort and time as we briefly discussed. A time dependent version of the streamline curvature method may deliver sufficiently accurate results for evaluating a dynamic simulation.

References

1. Schobeiri, M.T.: The Ultra-High Efficiency Gas Turbine Engine with Stator Internal Combustion, UHEGT. U.S. Patent Pending, 1389-TEES-99 (1999)
2. Schobeiri, M.T., Attia, S.: Advances in Nonlinear Dynamic Engine Simulation Technology. ASME 96-GT-392, presented at the International Gas Turbine and Aero-Engine Congress and Exposition, Birmingham, UK- June 10- 13 (1996)
3. Schobeiri, M.T., Abouelkheir, M., Lippke, C.: GETRAN: A Generic, Modularly Structured Computer Code for Simulation of Dynamic Behavior of Aero-and Power Generation Gas Turbine Engines, an honor paper. ASME Transactions, Journal of Gas Turbine and Power 1, 483–494 (1994)
4. Koenig, R.W., Fishbach, L.H.: GENENG- A Program for Calculating Design and Off-Design Performance for Turbojet and Turbofan Engines. NASA TN D-6552 (1972)
5. Seldner, K., Mihailowe, J.R., Blaha, R.J.: Generalized Simulation Technique for Turbojet Engine System Analysis. NASA TN D-6610 (1972)
6. Seller, J., Daniele, C.J.: DYGEN – A Program for Calculating Steady-State and Transient Performance of Turbojet and Turbofan Engines, NASA TND-7901 (1975)
7. Szuch, J.R.: HYDES- A Generalized Hybrid Computer Program for Studying Turbojet or Turbofan Engine Dynamics. NASA TM X-3014 (1974)
8. Agrawal, R.K., Yunis, M.: A Generalized Mathematical Model to Estimate Gas Turbine Starting Characteristics. Journal of Eng. Power 104, 194–201 (1982)
9. Schobeiri, M.T.: Aero-Thermodynamics of Unsteady Flows in Gas Turbine Systems. Brown Boveri Company, Gas Turbine Division Baden Switzerland, BBC-TCG-51 (1985)
10. Schobeiri, T.: COTRAN, the Computer Code for Simulation of Unsteady Behavior of Gas Turbines. Brown Boveri Company, Gas Turbine Division Baden Switzerland, BBC-TCG-53 (1985)
11. Schobeiri, T.: Digital Computer Simulation of the Dynamic Response of Gas Turbines. VDI-Annual Journal of Turbomachinery 1985, 381–400 (1985)
12. Schobeiri, T.: A General Computational Method for Simulation and Prediction of Transient Behavior of Gas Turbines. ASME-86-GT-180 (1986)
13. Schobeiri, T.: Digital Computer Simulation of the Dynamic Operating Behavior of Gas Turbines. Journal Brown Boveri Review 3, 87 (1987)
14. Schobeiri, T.: Digital Computer Simulation of the Dynamic Operating Behavior of Gas Turbines. Journal Brown Boveri Review 3, 87 (1987)
15. Schobeiri, H., Haselbacher, H.: Transient Analysis of Gas Turbine Power Plants Using the Huntorf Compressed Air Storage Plant as an Example. ASME-85-GT-197 (1985c)

16. Schobeiri, M.T., Attia, M., Lippke, C.: Nonlinear Dynamic Simulation of Single and Multi-spool Core Engines, Part I: Theoretical Method. AIAA, Journal of Propulsion and Power 10(6), 855–862 (1994)
17. Schobeiri, M.T., Attia, M., Lippke, C.: Nonlinear Dynamic Simulation of Single and Multi-spool Core Engines, Part II: Modeling and Simulation Cases. AIAA Journal of Propulsion and Power 10(6), 863–867 (1994)
18. Schobeiri, M.T.: Dynamisches Verhalten der Luftspeichergasturbine Huntorf bei einem Lastabwurf mit Schnellabschaltung. Brown Boveri, Technical Report, TA-58 (1982)